ENGINEERING HONORS PROGRAM
UNIVERSITY OF MICHIGAN

Engineering Honors Capstone: Final Report

Project: Synthetic Dry Adhesives for Human-Scaled Climbing of Vertical Surfaces

Student: William van den Bogert

Advisor: John Shaw

1 Summary

The goals of this project are summarized in three parts: (1) fabricate dry adhesives and characterize their performance, (2) demonstrate the feasibility of human-scale climbing with such adhesives, and (3) design, manufacture, and demonstrate an apparatus to allow humans to climb vertical glass or polished stone surfaces using these adhesives.

Throughout the Fall 2020 and Winter 2021 semesters a fabrication method for adhesives was devised, a testing setup was built, several performance tests were conducted on an *Instron* machine, and a climbing paddle for human use was designed and fabricated. The sizes of the adhesives tested were 100x150 mm (4x6 in) and 76x304 mm (3x12 in). The 100x150 mm pad was intended for pilot testing, while the 76x304 mm pad was the size designed for use in the climbing paddle.

For the pilot testing of the 100x150 mm pad, when force was applied parallel to the surface (the adhesive operated in shear), the maximum load held by the adhesive was 449 N (101 lbf), the minimum force capacity achieved was 139 N (31 lbf). From eleven shear tests, the average force capacity was 298 ± 16 N (67 ± 4 lbf). Nine more tests were performed, three with force applied normal to the surface (at 90°), three with force applied at an angle of 60° to the surface, and three with force applied at an angle of 30° to the surface.

For the testing of the 76x304 mm pad, the maximum load held by the adhesive was 448 N (101 lbf) and the minimum force capacity achieved was 293 N (66 lbf). From eight shear tests, the average force capacity was 389 ± 24 N (87 ± 5 lbf).

In pursuit of the third goal, this report also discusses a design for a climbing paddle that a human could use to scale vertical walls of suitable surface quality, most likely limited to glass and polished stone. Finite element analysis was performed on two designs of the main aluminum structure of the paddle, and the results can be found in this report. The results show that the structure should be suitable to support the weight of a human being. One climbing paddle weighs less than 5 lbf. The climbing paddle was then manufactured, but showed many shortcomings with respect to the assumptions made in its design.

2 Fabrication

The adhesive is a composite material, a carbon fiber-reinforced polyurethane matrix. The polyurethane is BJB Enterprises F-160, an elastomer with a Shore hardness of 60A. The carbon fiber is in the form of a 3K bi-directional plain weave fabric.

The adhesives were molded using a 3D printed mold with a borosilicate glass plate against which to mold the adhesive surface, seen in Figure 1 below.

Figure 1. Molding the adhesive with glass clamped on top.

Two layers of carbon fiber fabric as one will reinforce the adhesive surface while the other will form a stiff tendon through which the force exerted on the adhesive will be directed. These two layers are depicted in Figure 2. In the 76x304 mm adhesives for the climbing paddle, either two or four tendons were added.

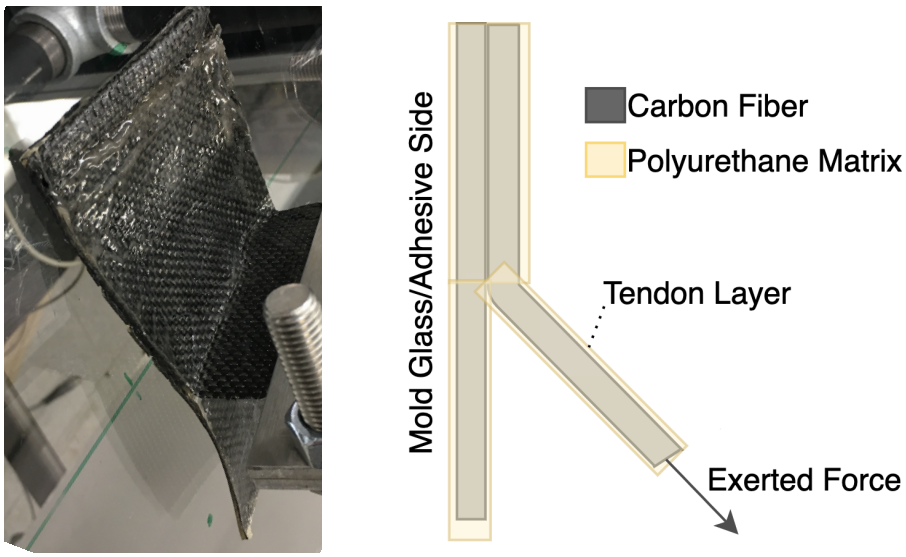

Figure 2. The two layers of the adhesive.

3 Testing

The *Instron* testing setup and the ability to test at multiple angles can be seen in Figure 3 below.

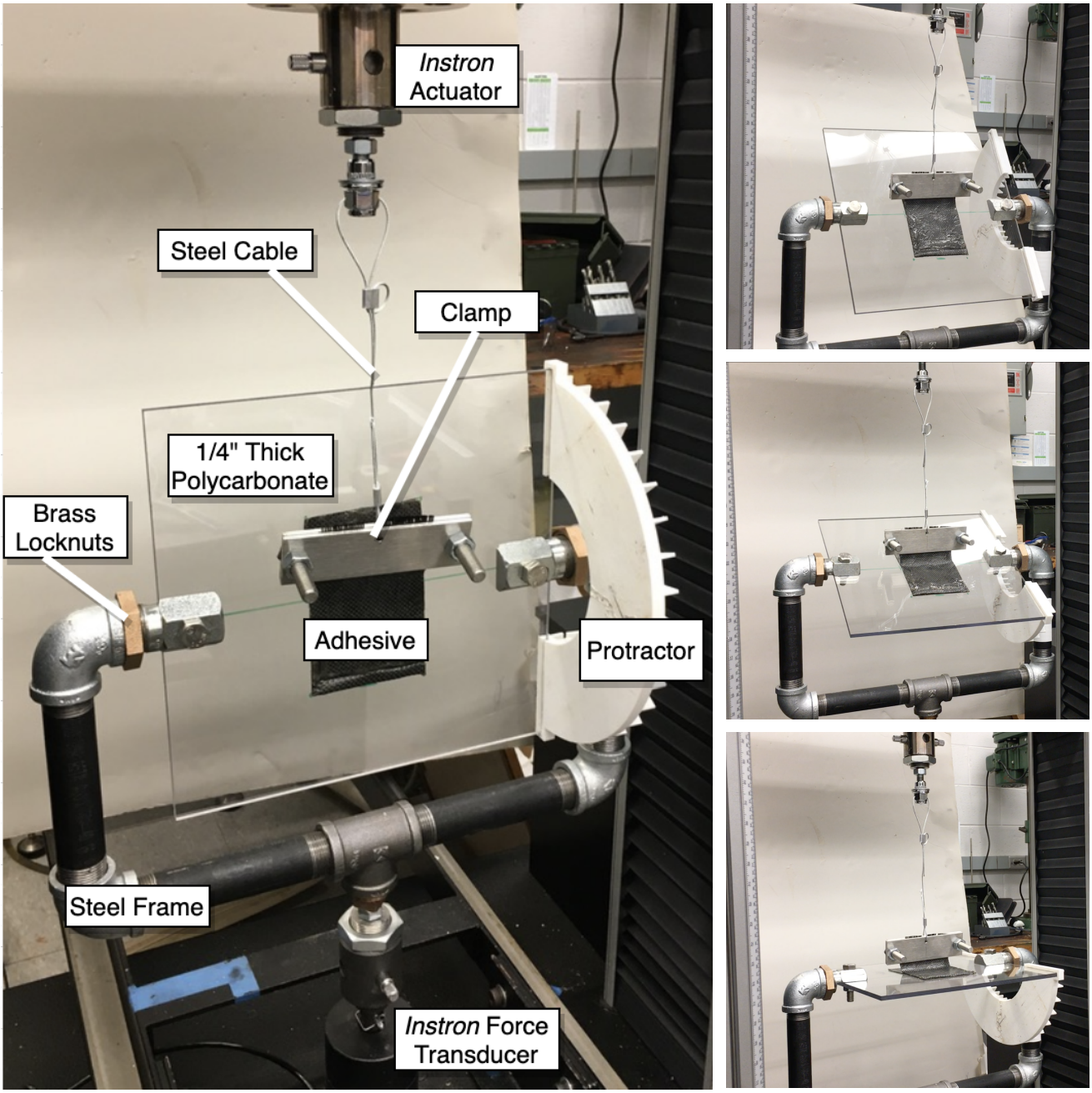

Figure 3. The testing setup in the 0° configuration (left), alongside 30°, 60°, and 90° configurations (right), with the 100x150 mm adhesive for the pilot tests included.

The *Instron* instrument was used to measure the force withstood by the adhesive as the actuator increased the displacement of the steel cable attached to the adhesive. The steel cable was attached to a clamp that held onto the tendon of the adhesive, and exerted a force as indicated in Figure 2.

A standard cleaning protocol for the adhesive was not decided upon during the pilot tests. Soap and water left a residue on the adhesive, which was not ideal. Cleaning the adhesive surface with isopropyl alcohol seemed to damage the surface of the polyurethane, and the potential decrease in smoothness was a concern, but after several tests indicated there was not a clear decline in adhesive force capacity after cleaning the adhesive with isopropyl alcohol, it was decided that this would be the standard cleaning protocol for the final tests. The cleaning protocol variable is not eliminated in the pilot tests, but is eliminated in the final tests.

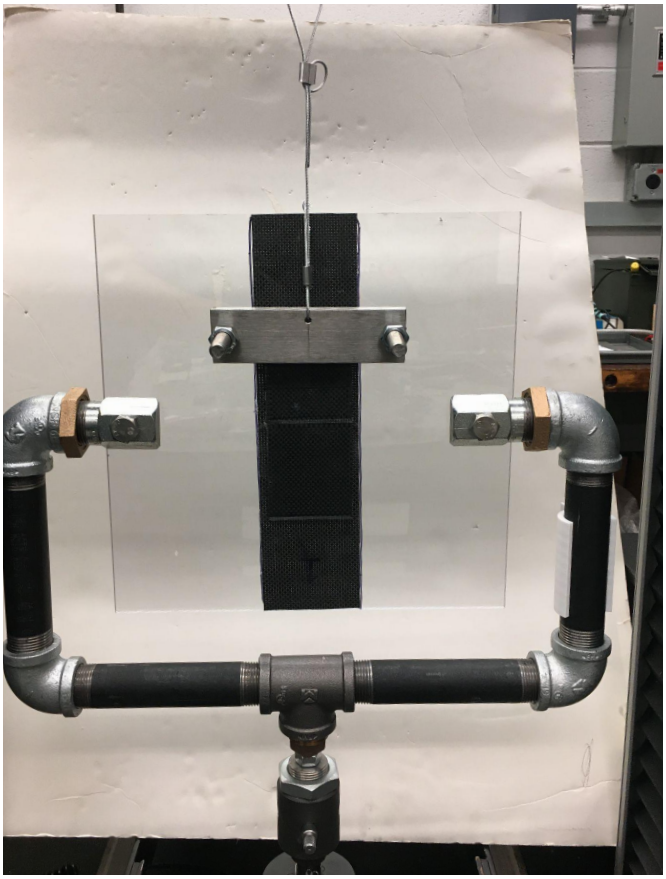

Figure 4. The 76x305 mm adhesive for the final tests placed in the testing setup.

4 Pilot Testing Results

After 20 tests were performed (11 for 0°, 3 for 30°, 3 for 60°, and 3 for 90° configuration) the data was analyzed to glimpse potential relationships between independent variables (test number and angle) and dependent variables (force capacity and compliance). Table 1 gives an overview of the test results. For tests 9 and 10, the adhesive was not removed and reattached after tests 8 and 9 respectively. All other tests involved removal and reattachment.

Table 1. Overview of pilot testing results

Test #	Method of Failure	Maximum Force Achieved (N)	Adhesive Pad Size	Angle (Degrees)
0	Adhesive Failure	355.67	100x150 mm	0
1	Adhesive Failure	264.26	100x150 mm	0
2	Adhesive Failure	364.08	100x150 mm	0
3	Adhesive Failure	139.56	100x150 mm	0
4	Clamp Failure	201.98	100x150 mm	0
5	Adhesive Failure	305.02	100x150 mm	0
6	Adhesive Failure	280.50	100x150 mm	0
7	Clamp Failure	284.93	100x150 mm	0
8	Load Cell Maximum Reached	449.35	100x150 mm	0
9	Clamp Failure	397.76	100x150 mm	0
10	Clamp Failure	236.20	100x150 mm	0
11	Adhesive Failure	176.79	100x150 mm	90
12	Adhesive Failure	53.55	100x150 mm	90
13	Adhesive Failure	91.29	100x150 mm	90
14	Adhesive Failure	80.40	100x150 mm	60
15	Adhesive Failure	70.40	100x150 mm	60
16	Adhesive Failure	61.38	100x150 mm	60
17	Adhesive Failure	149.95	100x150 mm	30
18	Adhesive Failure	139.46	100x150 mm	30
19	Adhesive Failure	135.76	100x150 mm	30

4.1 Effect of test number on adhesive performance

Tests 0–19 were conducted in numerical order, such that the performance of the adhesive as these tests continue also potentially show how the performance changes over time and over several cycles. Figures 5 and 6 show the results of this analysis.

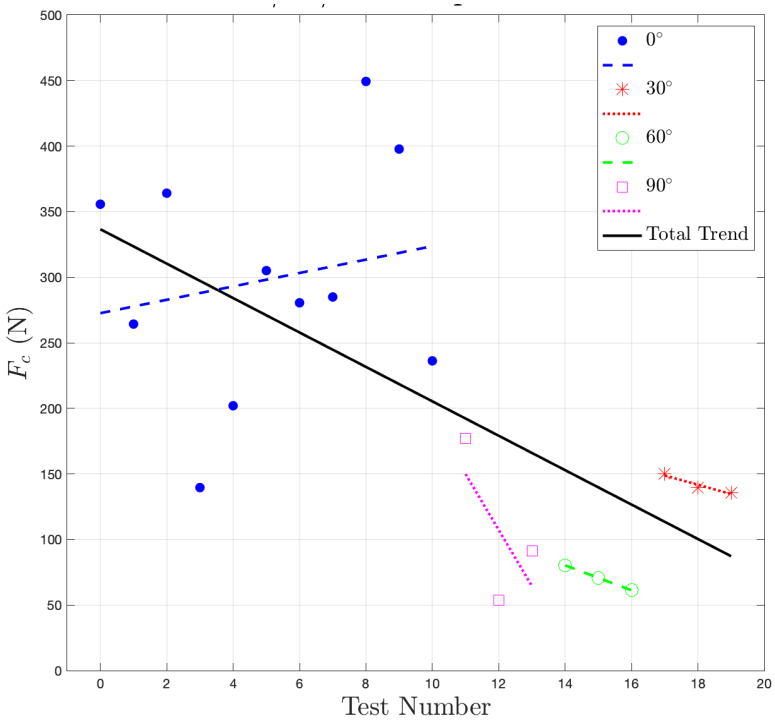

Figure 5. The force capacity in Newtons plotted for tests 0–19. The angle for each test is also indicated. The total trend might indicate that the force capacity decreases over time or over cycles, but the angle might also affect the force capacity. The slope of the 0° trendline (blue) is 5.107 ± 20.013. Because the 95% confidence interval includes 0, no relationship between time or cycles and adhesive performance is apparent at this time. Not enough data was acquired in the other angles to interpret those trendlines meaningfully. It is still quite possible that the adhesive performance declines with time or repeated cycles, but it likely takes far more than 11 cycles to see this effect.

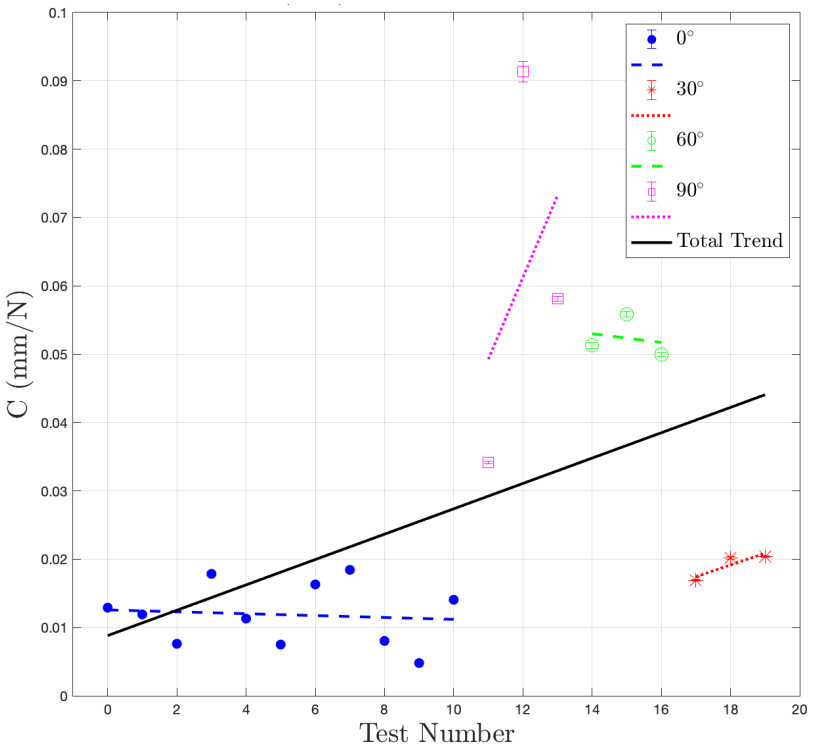

Figure 6. The compliance of the adhesive in mm/N plotted for tests 0–19. The compliance is the reciprocal of the slope of the linear region of the force vs. extension plots, as seen in Appendix A. In a similar manner to Figure 4, the total trendline here is misleading as the angle may affect the compliance. The slope of the 0° trendline (blue) is -0.0001386 ± 0.0010274. The confidence interval again includes 0, so no relationship between compliance and number of cycles is observed here.

4.2 Effect of angle on adhesive performance

The angle at which the force was applied to the adhesive appeared to have a significant effect on the force capacity and the compliance, as seen in Figures 6 and 7.

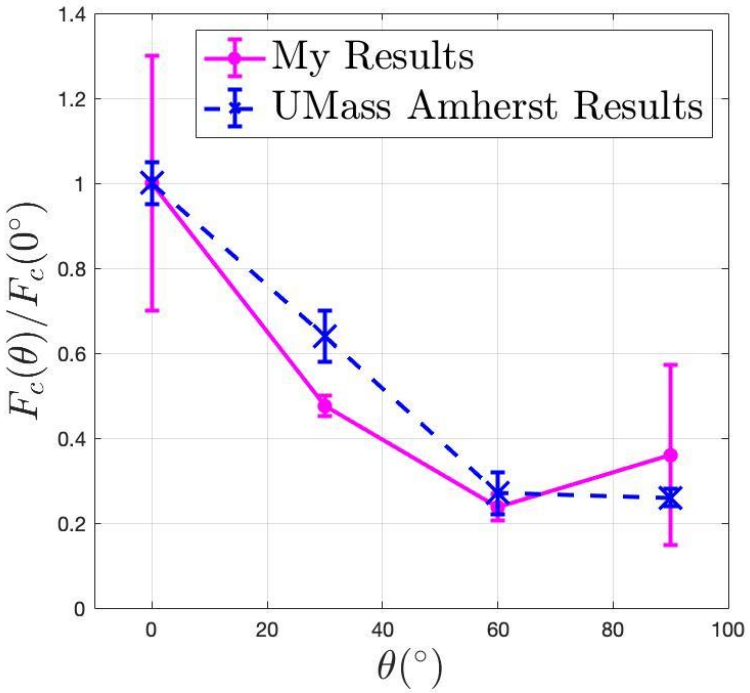

Figure 7. The average force capacities (as a ratio to the shear force capacity) and precision error plotted for each test angle. For the most part, the force capacity appears to decrease as the angle increases. This is consistent with the findings of UMass Amherst [1], as shown here.

5 Preliminary Climbing Apparatus Design

Bartlett et al. [2] developed a mathematical model for adhesives made from fiber reinforced elastomers, such as the ones explored in this project. They propose a scaling theory that relates the force capacity F_c of an adhesive pad to the area A and compliance C of that pad, as shown in Equation 1.

$$F_c \sim \sqrt{\frac{G_c A_c}{C}} \tag{1}[2]$$

Bartlett et al. [2] also proposed a theory for how this is affected when multiple adhesive pads act in parallel. Equation 2 shows how the compliances of each pad add inversely, where C_{total} is the combined compliance of all the pads, N is the number of pads, and C_i is the compliance of a single pad, assuming they are all identical.

$$C_{total} = \sum_{j=1}^{N} \frac{1}{C_j} = \frac{C_i}{N} \tag{2}[2]$$

By contrast, the total contact area scales with the number of pads, as shown in Equation 3, where A_{total} is the total contact area, N is the number of pads, and A_i is the contact area of a single pad, assuming they are all identical.

$$A_{total} = \sum_{j=1}^{N} A_j = A_i N \quad (3)[2]$$

From Equation 2 and Equation 3, it can be shown that the force capacity of multiple adhesive pads arranged in parallel scales with the number of pads, as in Equation 4.

$$F_c \sim \sqrt{\frac{G_c(A_i N)}{(C_i/N)}} \sim N \cdot \sqrt{\frac{G_c A_i}{C_i}} \quad (4)[2]$$

In comparing a single large adhesive pad with contact area A, and a set of N smaller pads each of area A_i such that both configurations took up the same amount of area, that is to say $A_i N = A_{total} = A$, we would find that they are evaluated differently, as shown in Equations (5) and (6), where $F_{c,single}$ is the force capacity of the single large pad and $F_{c,multiple}$ is the force capacity of the multiple pad system.

$$F_{c,single} \sim \sqrt{\frac{G_c A}{C}} \quad (5)[2]$$

$$F_{c,multiple} \sim \sqrt{\frac{N G_c A}{C_i}} \quad (6)[2]$$

The criterion for $F_{c,multiple}$ being an improvement over $F_{c,single}$ is shown in Equation 7.

$$F_{c,multiple}/F_{c,single} = \sqrt{\frac{NC}{C_i}} > 1 \quad (7)[2]$$

Essentially, this shows that there will be an improvement so long as the compliance of a small pad is not greater than the compliance of the large pad by a factor of N. In other words, the compliance of the small pad must be minimized, while reducing the area of the pad to A/N. The compliance will generally decrease as the height of the pad increases, as shown by Equation 8:

$$C \approx \frac{1}{\mu b}\left(\left(\frac{t}{h}\right) + \frac{4}{3}\left(\frac{t}{h}\right)^3\right) \quad (8)[2]$$

So keeping the pads tall, and oriented with their long axes parallel to the load should help the performance of the adhesive. This is the idea behind the design presented below.

5.1 Preliminary Adhesive Climbing Paddle Design

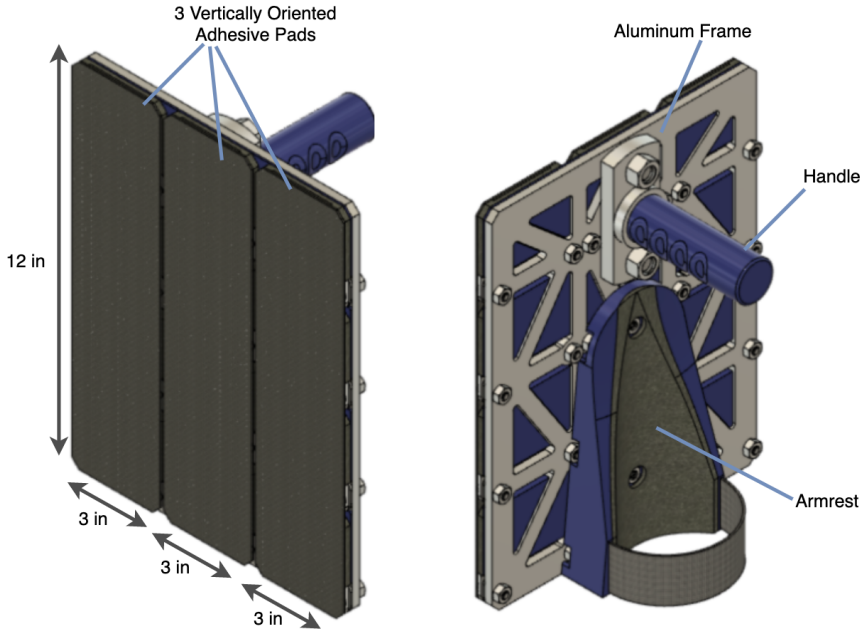

Figure 8. The preliminary design for one climbing paddle. The user would have one on each arm. One paddle alone should support a human being.

The design shown in Figure 15 has three pads, each 12in by 3in in size. The combined area of these pads is 108 in^2 or about 0.07 m^2. This is about 4.6 times the area of the adhesive used in the experiments discussed above. Not knowing the compliances of these pads, and assuming that the adhesive force scales by area, the force capacity of these pads could be 4.6 times the above 0° experiments' average of 298 N, about 1371 N or 308 lbf.

The assumption that adhesive force scales by area is informed by Equation 8. If the ratio between thickness and height *t/h* is small, as is the case with the adhesives in question, then the $(t/h)^3$ term can be ignored in favor of the $(t/h)^1$, such that the compliance C is inversely proportional to the area A or $C \sim 1/A$. This means that the relation $F_c \sim \sqrt{A/C}$ can be approximated by $F_c \sim A$.

The weight estimates from Autodesk Fusion 360 are quite rough, especially considering the 3D printed parts will be less dense, but the program estimates a single paddle will weigh about 4.7

lbf. A different frame shape option could lower the weight to 4.3 lbf. These two frames are shown in Figure 16.

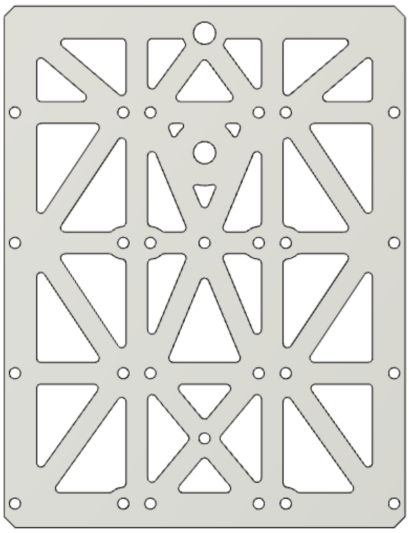

Sturdy: 0.5” thick members: Climbing paddle weighs 4.7 lbf

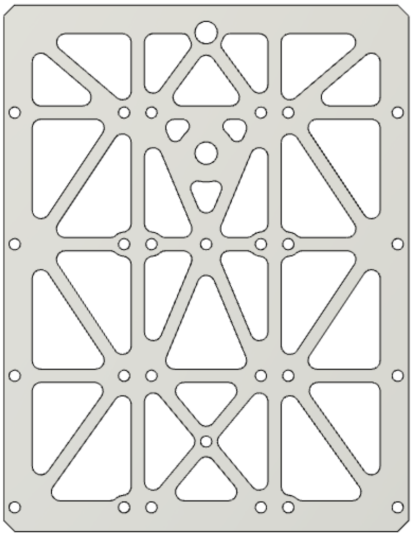

Light: 0.3” thick members: Climbing paddle weighs 4.3 lbf

Figure 9. Two possible versions of the climbing paddle frame.

Finite element analysis was performed to confirm that either frame is capable of supporting 1300N or around 300 lbf downware at the handle, with the effects of bending included. These results are shown in Figure 17 below.

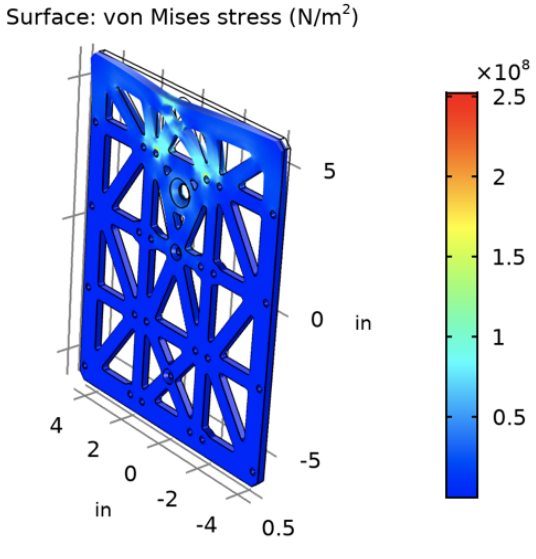

Sturdy: 0.5” thick members: Climbing paddle weighs 4.7 lbf

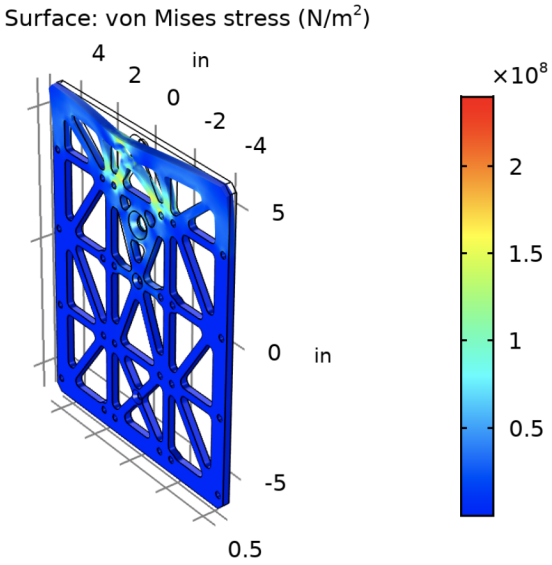

Sturdy: 0.5” thick members: Climbing paddle weighs 4.7 lbf

Figure 10. Finite element analysis of each plate supporting around 300 lbf. The yield strength of 6061 Aluminum is around 276 MPa, so these should be fully capable of supporting a <200 lb person.

Each adhesive pad has four tendons attached to it, as shown in Figure 18. This helps to keep the pad oriented approximately parallel to the paddle in order to ensure ease of placement on a wall (a single tendon pad would bend over under its own weight, and a pad rigidly attached to the pad will not have the force properly directed into a tendon) and distribute to force to four discrete locations that are not the edges of the pad, preventing peeling at the edges. Each tendon is clamped by aluminum jaws so that they are fixed to the aluminum frame.

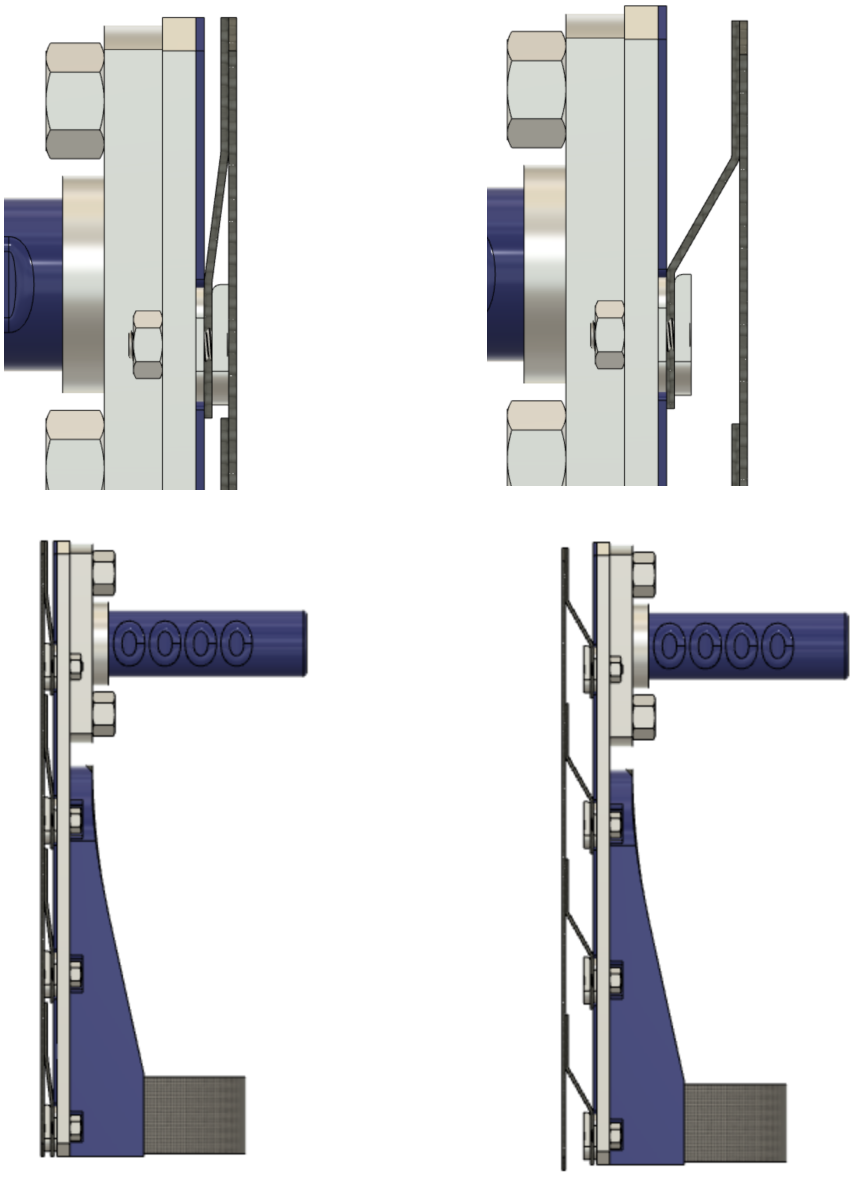

Figure 11. The use of multiple tendons is a compromise between a rigid pad (which will not properly conform to the surface) and a loose pad (which will be difficult to place on a surface).

Low-density polyurethane foam makes up a spongy layer between the aluminum frame and the adhesive pad. This dampens the act of placing the paddle on a surface, and exerts a force onto the adhesive pad so that it is forced against the surface as long as the adhesive is sufficiently supporting the weight, the compression of these foam pads during placement can be seen in Figure 19.

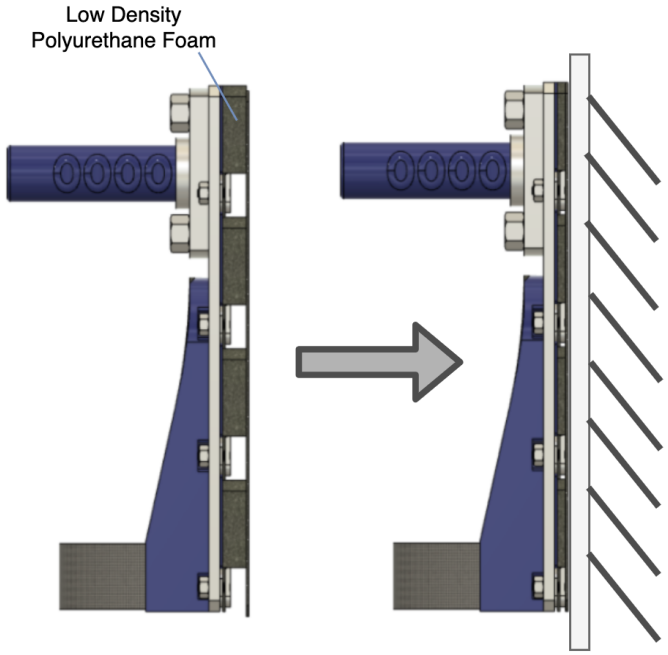

Figure 12. Compression of foam elements during placement. Essentially, this is a transition from compressive elements (foam) to tensile elements (tendons) acting on the wall.

Before final testing, it was hypothesized that constraining the adhesive through four tendons would introduce weak points at the top and bottom of the adhesive pad. Thus, adhesive pad Samples 1 and 3 were only fabricated with tendons near the center for testing, as detailed in section 6. This hypothesis was supported by the testing of Sample 4, outlined in section 6.3.

6 Final Adhesive Testing

After completing the designs discussed above, the performance of one of the 76x305 mm adhesive pads with four tendons was tested using the same methods outlined in section 3, with similar results to section 4 being reported. As the purpose of this testing was to show that human

climbing using the above design was feasible, the adhesive was only tested in shear, i.e. pulling angles other than 0° as presented in Figure 7 were not investigated. Only loading one tendon out of the four was possible at a time. Table 2, in which the tendons are numbered according to Figure 13, gives an overview of these test results.

Figure 13. The tendon numbering convention for the following results.

Table 2. Overview final pilot testing results

Sample Number	Loaded Tendon	Test #	Method of Failure	Maximum Force Achieved (N)	Adhesive Pad Size (mm)	Angle (Degrees)
1	2	1	Clamp Failure	296.78	76x305	0
1	2	2	Partial Peel	372.72	76x305	0
1	2	3	Partial Peel	447.95	76x305	0
1	2	4	Partial Peel	447.09	76x305	0
1	2	5	Partial Peel	293.49	76x305	0
1	2	6	Partial Peel	359.16	76x305	0
1	2	7	Partial Peel	447.13	76x305	0
1	2	8	Partial Peel	446.12	76x305	0
1	3	1	Full Peel	247.22	76x305	0

1	3	2	Full Peel	390.11	76x305	0
1	3	3	Clamp Failure	424.50	76x305	0
1	3	4	Full Peel	368.73	76x305	0
1	3	5	Partial Peel	388.86	76x305	0
1	3	6	Clamp Failure	349.53	76x305	0
1	3	7	Partial Peel	366.43	76x305	0
3	2	1	Clamp Failure	255.84	76x305	0
3	2	2	Clamp Failure	260.59	76x305	0
3	2	3	Full Peel	221.47	76x305	0
3	2	4	Clamp Failure	234.28	76x305	0
3	2	5	Clamp Failure	283.42	76x305	0
3	3	1	Full Peel	287.35	76x305	0
3	3	2	Full Peel	251.17	76x305	0
3	3	3	Full Peel	293.89	76x305	0
4	1	1	Full Peel	194.19	76x305	0
4	2	2	Full Peel	371.88	76x305	0
4	3	3	Full Peel	229.30	76x305	0
4	4	4	Full Peel	32.45	76x305	0

6.1 Testing of the highest quality sample

Sample 1 was the highest quality adhesive pad fabricated. It can be visually compared to Samples 3 and 4 in Appendix D. The results from testing the lower, centermost tendon (Tendon 2) can be seen in Figure 14 below.

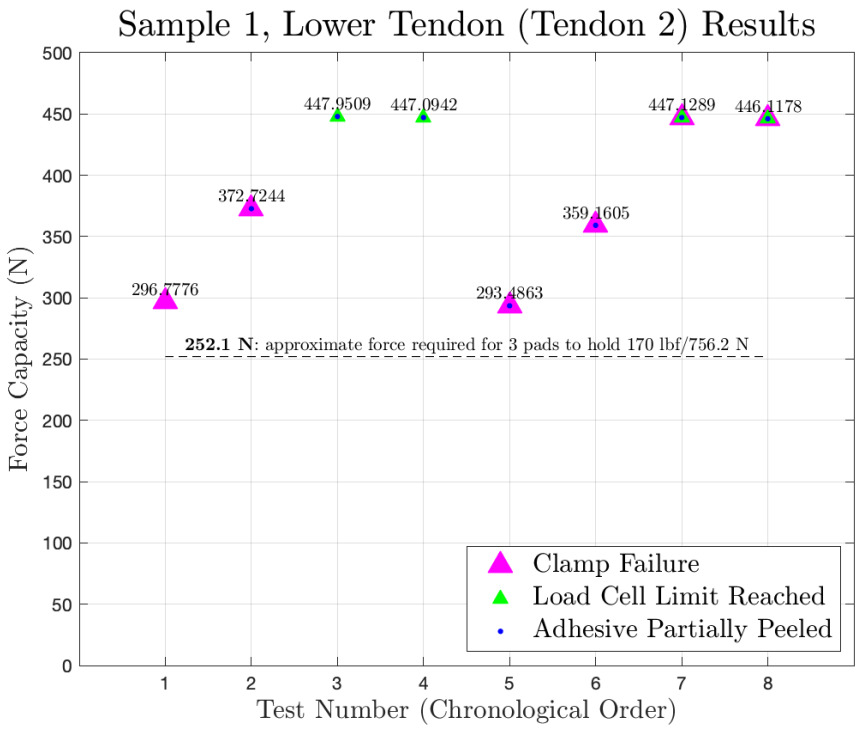

Figure 14. Results from loading Tendon 2 on Sample 1. As shown, all eight adhesive tests show critical loads higher than that required for three pads to hold a human being's weight of 170 lbf while acting in parallel, as in the design outlined in section 5.

Loading the upper tendon (Tendon 3) for Sample 1 was shown to be slightly weaker, with all but one test showing support for the climbing paddle design, as seen in Figure 15 below.

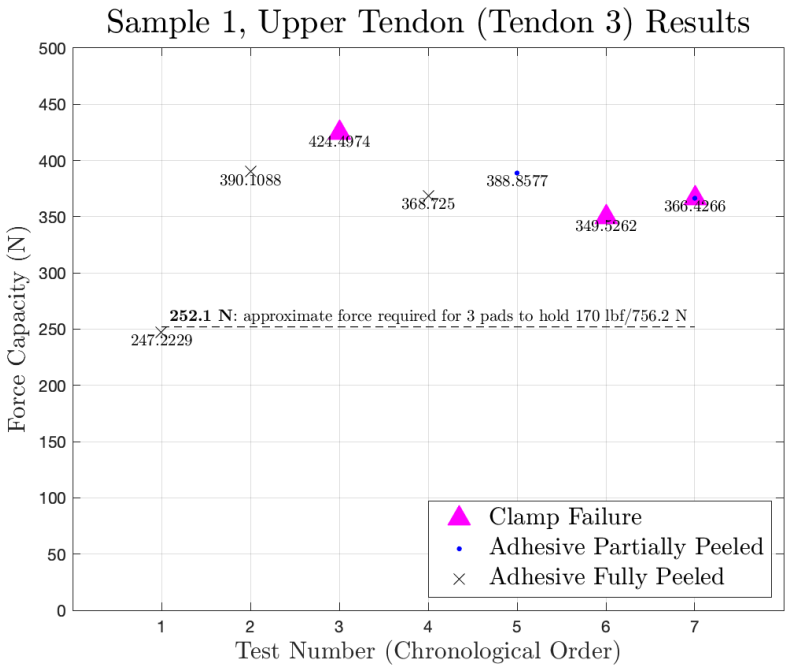

Figure 15. Results from loading Tendon 3 on Sample 1. As shown, six of the seven adhesive tests show critical loads higher than that required for three pads to hold a human being's weight of 170 lbf while acting in parallel, as in the design outlined in section 5. This indicates that the upper tendon may be a weak point.

6.2 Testing of a lower quality sample

Sample 3 was of lower quality than Sample 1, with more fabrication defects as can be seen in Appendix D. This sample only showed a handful of tests wherein the adhesive force capacity was high enough such that the design outlined in section 5 would function as intended, however the tendons were of lower quality as well, leading to many clamp failures. The results can be seen in Figure 16 below.

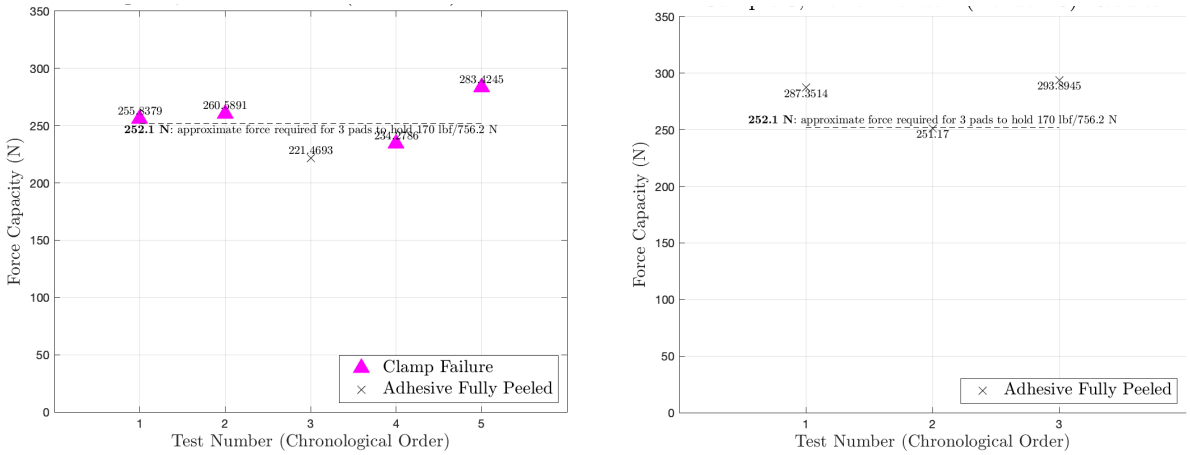

Figure 16. Results from loading Tendon 3 (left) and Tendon 2 (right) on Sample 3. This adhesive showed worse performance than Sample 1, which could be caused by its lower surface quality.

6.3 Testing tendons at differing locations

Sample 4 was also of lower quality than Sample 1, as can be seen in Appendix D. This sample was fabricated with four tendons as in the preliminary design, in order to support the hypothesis that Tendons 1 and 4 provide a weak point to the adhesive. The results for testing each tendon are shown in Figure 17 below.

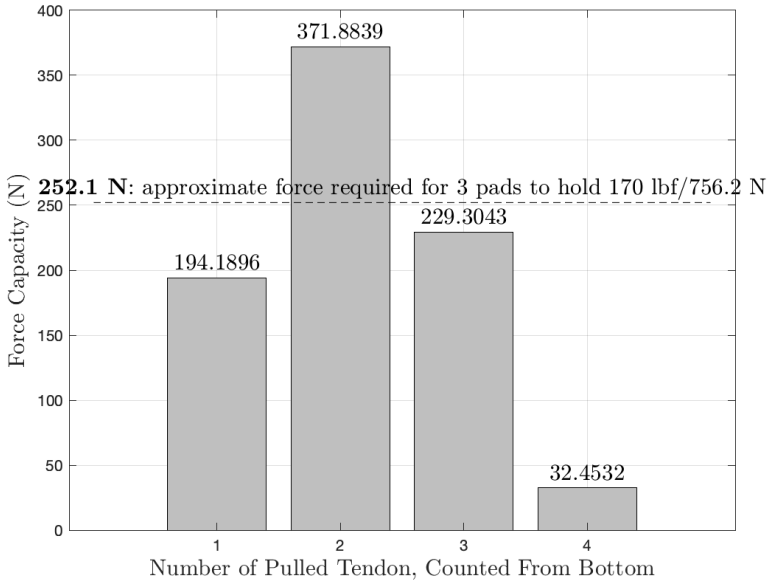

Figure 17. The results from loading Tendons 1–4 on adhesive Sample 4. This supports the hypothesis that loading the tendons farthest from center attachment (1,3,4) prevents higher critical loads, with the highest tendon (4) almost eliminating the load-bearing abilities of the adhesive.

6.4 Validation of the scaling theory

As all of the data collected throughout both the pilot and final tests includes both force capacity and compliance, and as the area is known, it was possible to assess the validity of the scaling theory from Bartlett et al [2], presented in section 5. The results of this characterization can be seen in Figure 18 below.

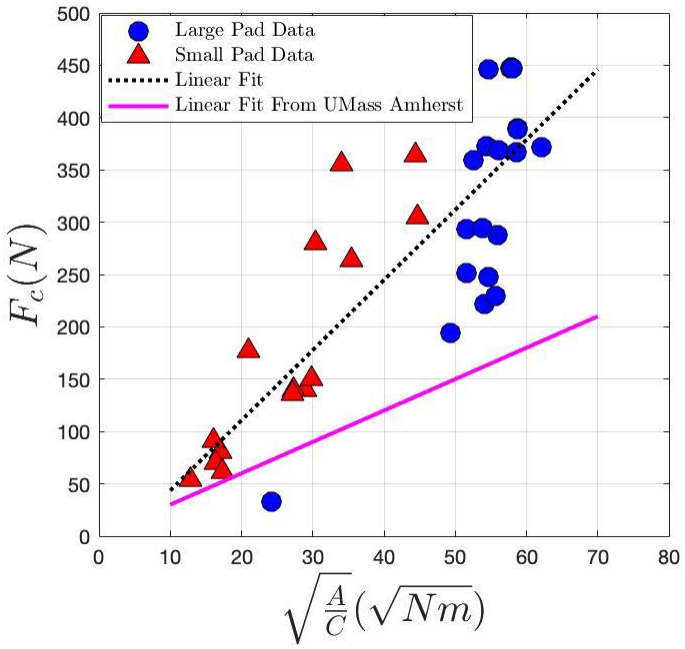

Figure 18. The force capacity is plotted with respect to the quantity of the square root of the ratio between adhesive pad area and the compliance, as measured throughout both the pilot testing (small pad data) and the final testing (large pad data).

A linear relationship can be seen, supporting the idea that van der Waals-powered adhesion can be modeled with this theory. However, the slope derived from this project's experiments is significantly higher than the slope derived from the experiments from Bartlett et al [2], even with similar materials used. This could be explained by the use of polycarbonate as the adherend surface, a much more compliant material than the glass used in the experiments from Bartlett et al [2]. That is to say the compliance measured in these experiments is not the true compliance of the adhesive.

8 Design Modifications and Manufacturing

From the observations made in the testing of Sample 4 in section 6.3, it was chosen to eliminate the uppermost and lowermost tendons of the four tendons in the preliminary design. Instead only two levels of clamps would be used. This allowed for the aluminum frame to be truncated at the corners, and have the material replaced by 3D-printed plastic, such that the rectangle shape is

maintained to compress the foam into the adhesive pads. This new design can be seen in Figure 19 below.

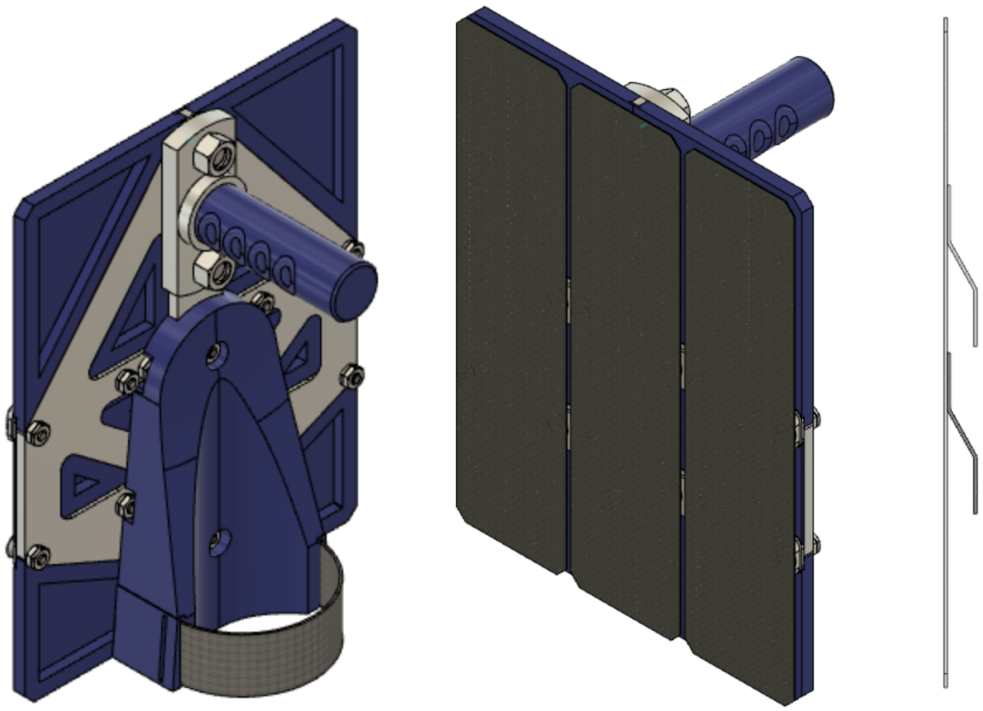

Figure 19. The new paddle design and a side view of the new adhesive pad with two tendons.

Additionally an aluminum bar was introduced along the back of the aluminum frame as reinforcement, as shown in Figure 20 below.

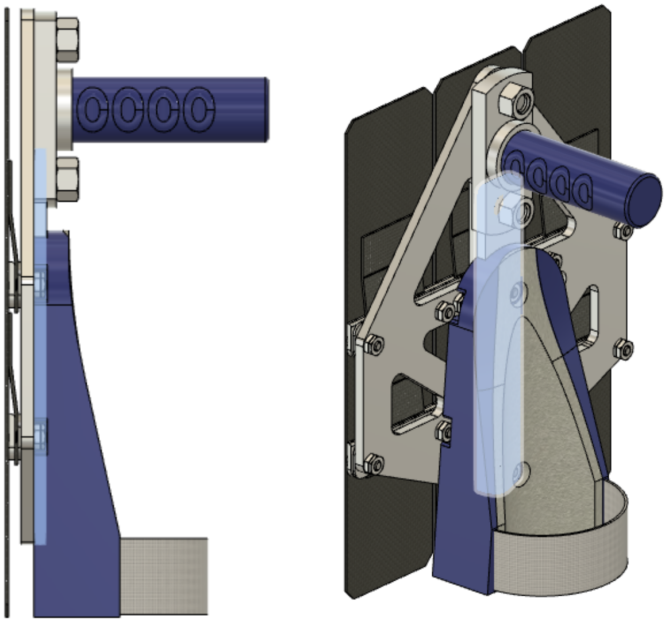

Figure 20. The location of the aluminum reinforcement bar.

Once this design was finished, it was manufactured using the waterjet at the Mechanical Engineering Machine Shop, and manually milled at the Wilson Student Team Project Center. The manufactured climbing paddle can be seen in Figure 21 below.

Figure 21. The fully manufactured climbing paddle.

9 Climbing Paddle Testing

It was verified that the force capacity of the entire climbing paddle was somewhere between 50 N and the human weight of 756.2 N. A spring scale exerting 50N at the handle was not enough to cause the paddle to fail but a human pulling down on the handle from directly below it did cause the adhesive to fail. The testing of both is seen in Figure 22.

Figure 22. Testing the adhesive pad with both 50N (left) and human weight (right) loads.

The adhesive pad appears to “tip” away from the glass surface as a force is applied to the handle, as shown in Figure 23. This is likely due to the force being applied at some lever arm away from the surface, creating a moment.

Figure 23. The tipping of the adhesive pad away from the adherend surface due to an applied moment.

Figure 24 shows an attempt to mitigate this tipping moment by mounting all three adhesives by only one tendon, onto an upside-down climbing paddle, such that the handle is at the bottom. The climbing paddle still fails.

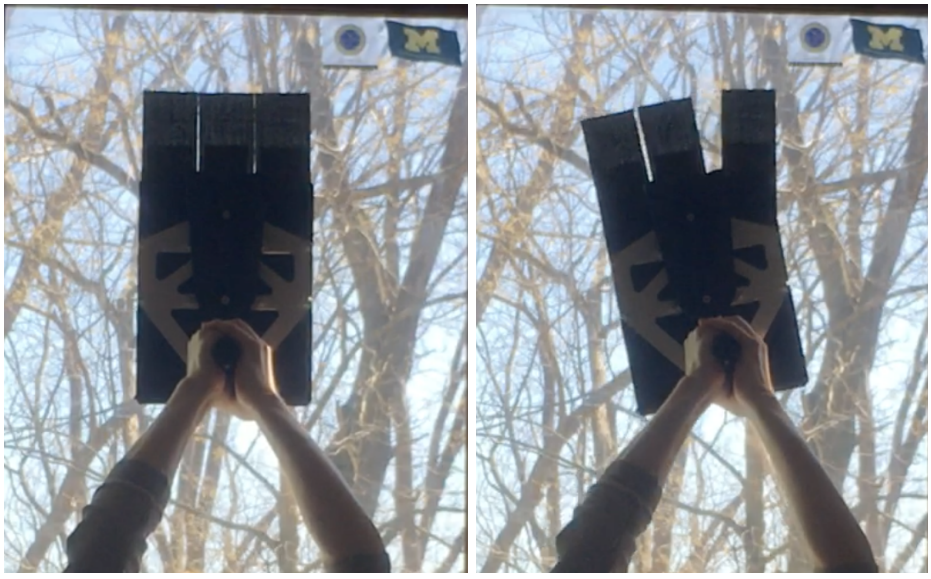

Figure 24. Failure of the climbing paddle, even after the handle is rearranged toward the bottom.

10 Discussion and Future Plans

From the pilot experiments conducted on the 100x150mm sample adhesive, and the relative size of the proposed climbing paddle design, it was clear to see that feasibility of human climbing with such adhesives had been demonstrated. However, unpredictability was also demonstrated. At its best, the 100x150mm sample performed with a force capacity of 449 N, and at its worst, a mere 139 N.

The final testing experiments included a regular cleaning protocol for the adhesives, and the fabrication of the 76x305 mm adhesive samples was better controlled, and the defects were largely eliminated. This led to more predictability, with the highest quality sample performing with a maximum force capacity of 448 N, and a minimum force capacity of 293 N. Additionally, the testing of the 76x305 adhesive samples still supported the hypothesis that the climbing paddle design would work, given three assumptions: (1) The three adhesive pads are loaded perfectly in parallel, and share the load equally, (2) any one adhesive pad is loaded in the same way as in the testing setup, and (3) all of the adhesive pads attached to the paddle are high quality.

The testing of the fully fabricated climbing paddle suggested that these assumptions do not hold. Figure 24 shows the failure of the climbing paddle, but one adhesive pad remains on the surface. This could suggest that the three pads are not loaded perfectly in parallel, and the one remaining on the surface was not holding its equal share of the load. The clamping system as design also does not provide any assurance that all the tendons are loaded in parallel, either. Thus, the first assumption that the three adhesive pads are sharing the load equally in parallel does not hold.

Figure 23 shows the climbing paddle failure due to a tipping moment being applied at the handle. This moment seems to cause the upper tendon to fail first, indicating that it is bearing most of the load. As shown in section 6.3, the upper tendon is a weak point, and is not capable of holding the required load on its own. This tipping also may load the upper tendon at a much higher angle than 0° to the surface, as opposed to being operated close to shear. As shown in section 4.2, these types of loading angles significantly decrease the adhesive's force capacity. Thus, the second assumption that the adhesive pad is loaded the same way as in the testing setup does not hold.

The third assumption clearly does not hold, as the only sample without defects is Sample 1. But it may not matter. As shown in section 6.6, the force capacity of Sample 4 when loaded at Tendon 3, which had many defects as can be seen in Appendix D, was comparable to that of Sample 1 when loaded at Tendon 3. Thus the defects are most likely not the main problem with the adhesive performance.

The adhesives demonstrated by Bartlett et al were of a similar size to those demonstrated here, but reached force capacities of around 3000 N, as opposed to a mere 400 N [2]. So something could be fundamentally wrong with the fabrication or design of these adhesives as presented in this report. As can be seen in Figure 18, the adhesives presented here follow a similar, if not better, scaling than those presented by Bartlett et al. And, as this report presents adhesives that have similar areas to those demonstrated there, then the main problem preventing higher critical loads is likely that the adhesives presented here are too compliant. It is then the recommendation of this report that the first step toward improving the performance of these adhesives is to reduce the compliance.

As for improving the design of the climbing paddle, a foothold could be implemented in order to mitigate the tipping moment further, attached by a long cable to the climbing paddle, to ensure the adhesives are being loaded in shear. A mechanism could also be added to equalize the tension in the tendons, ensuring that all the adhesives are sharing the load equally.

As this was a self-funded project, there are currently no future plans, only suggestions and ideas, to continue this work. Should this project be taken on by another group, these suggestions will serve them well.

11 References

[1] Bartlett, M. D., Croll, A. B., King, D. R., Paret, B. M., Irschick, D. J., & Crosby, A. J. (2012). Looking beyond fibrillar features to scale gecko-like adhesion. *Advanced materials (Deerfield Beach, Fla.)*, *24*(8), 1078–1083.

[2] Bartlett, M.D., Croll, A.B. and Crosby, A.J. (2012), Designing Bio‐Inspired Adhesives for Shear Loading: From Simple Structures to Complex Patterns. Adv. Funct. Mater., 22: 4985-4992.

Appendix A: Force vs. Extension Plots for Pilot Tests (100x150 mm pad)

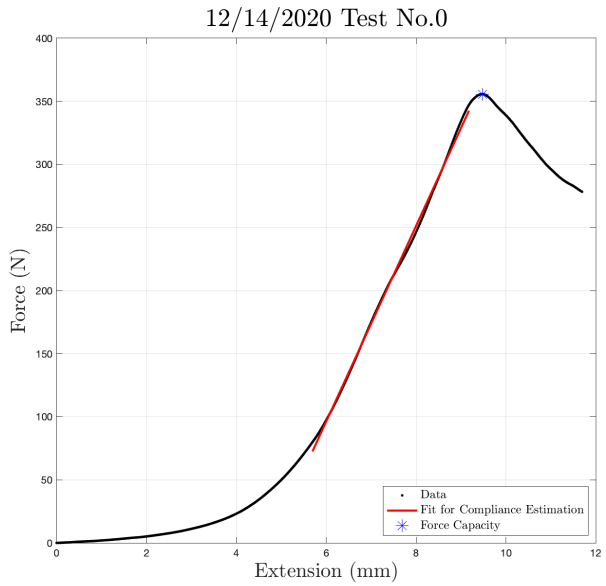

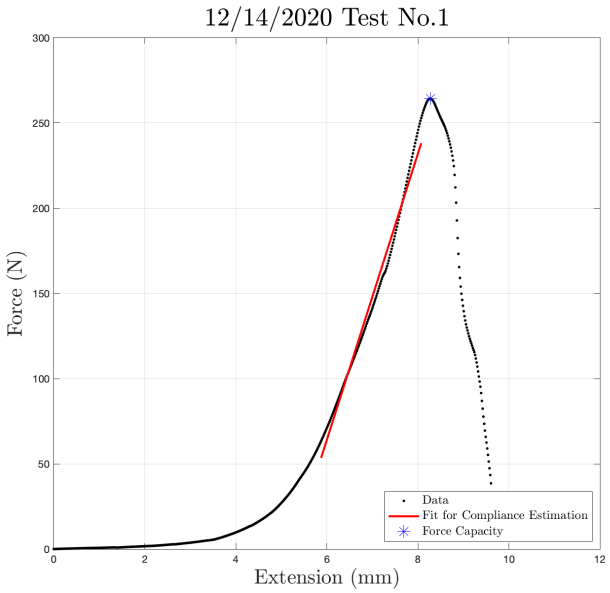

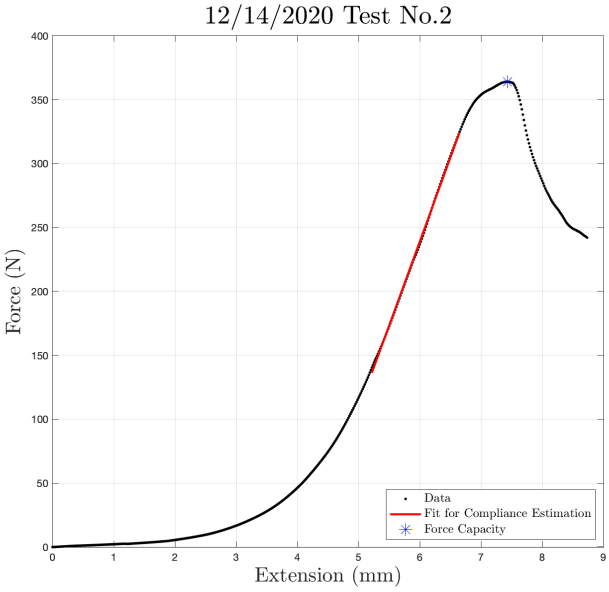

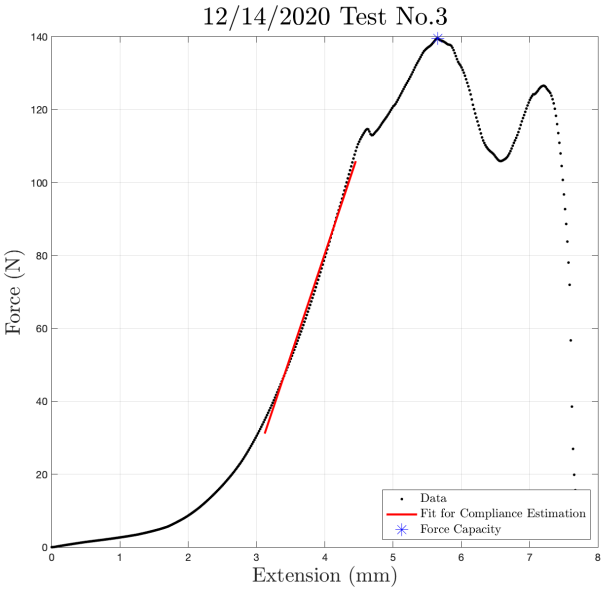

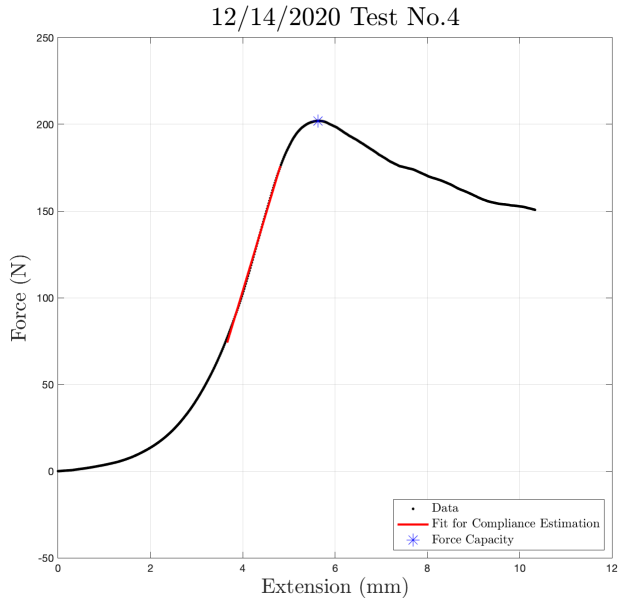
12/14/2020 Test No.4
Force (N)
Extension (mm)
Data
Fit for Compliance Estimation
Force Capacity

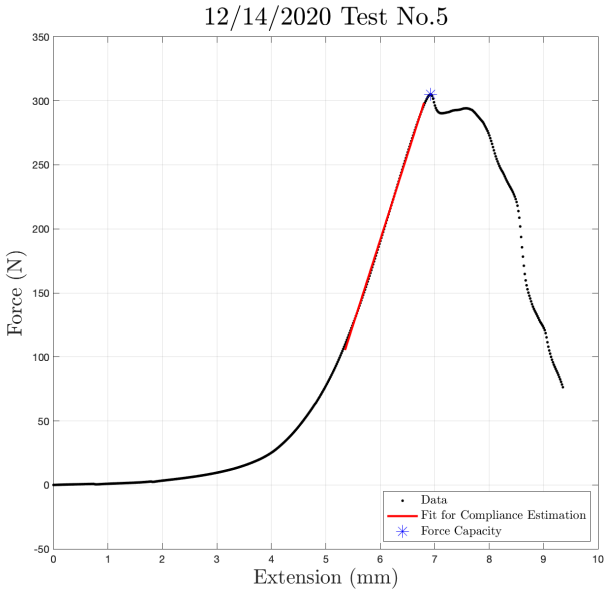
12/14/2020 Test No.5
Force (N)
Extension (mm)
Data
Fit for Compliance Estimation
Force Capacity

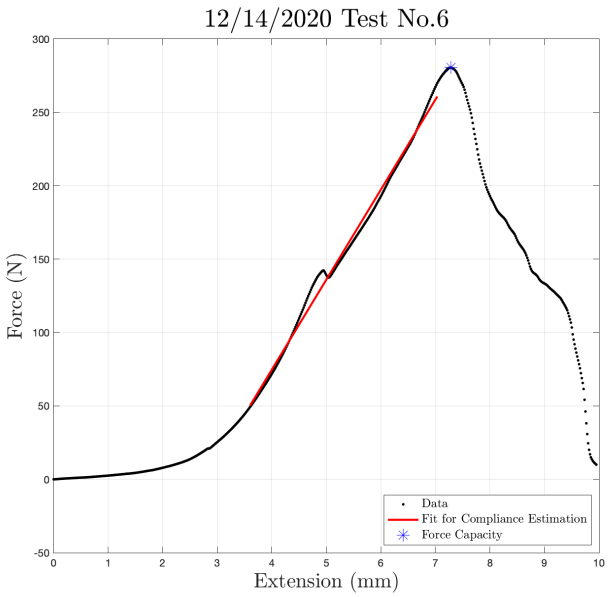
12/14/2020 Test No.6
Force (N)
Extension (mm)
Data
Fit for Compliance Estimation
Force Capacity

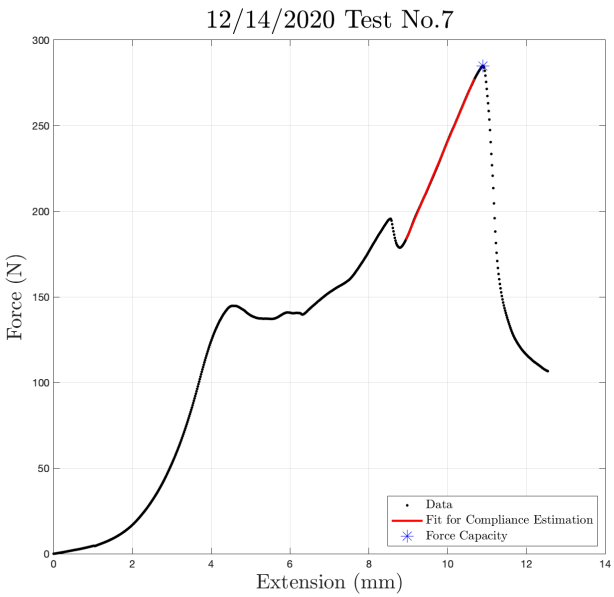
12/14/2020 Test No.7
Force (N)
Extension (mm)
Data
Fit for Compliance Estimation
Force Capacity

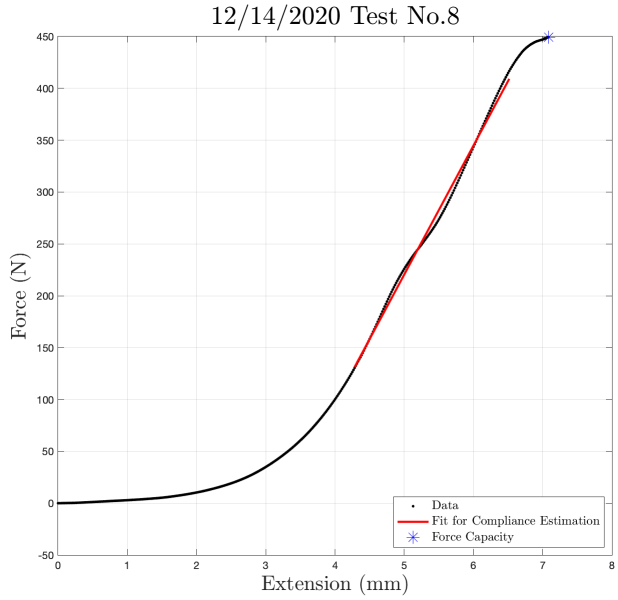
12/14/2020 Test No.8
Force (N)
Extension (mm)
Data
Fit for Compliance Estimation
Force Capacity

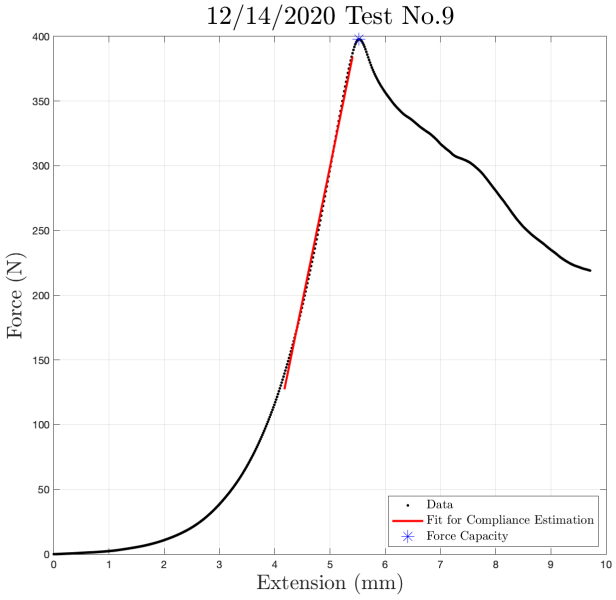
12/14/2020 Test No.9
Force (N)
Extension (mm)
Data
Fit for Compliance Estimation
Force Capacity

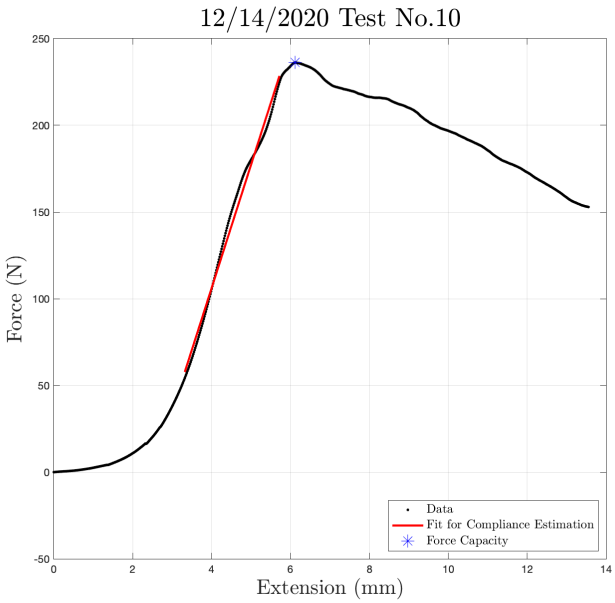
12/14/2020 Test No.10
Force (N)
Extension (mm)
Data
Fit for Compliance Estimation
Force Capacity

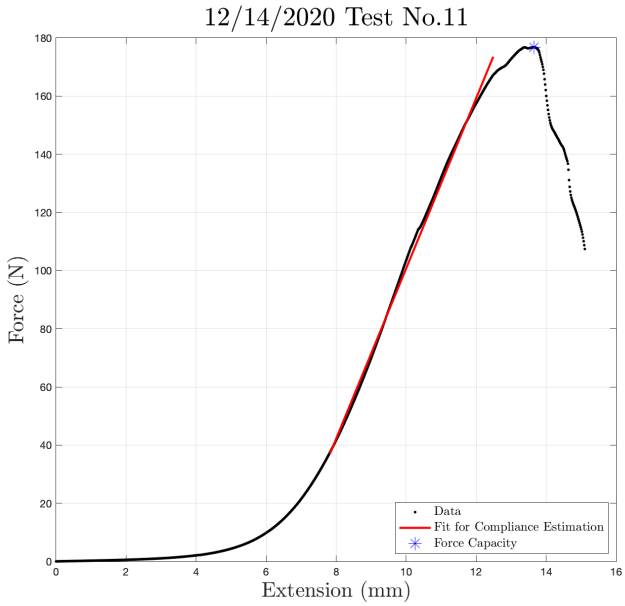
12/14/2020 Test No.11
Force (N)
Extension (mm)
Data
Fit for Compliance Estimation
Force Capacity

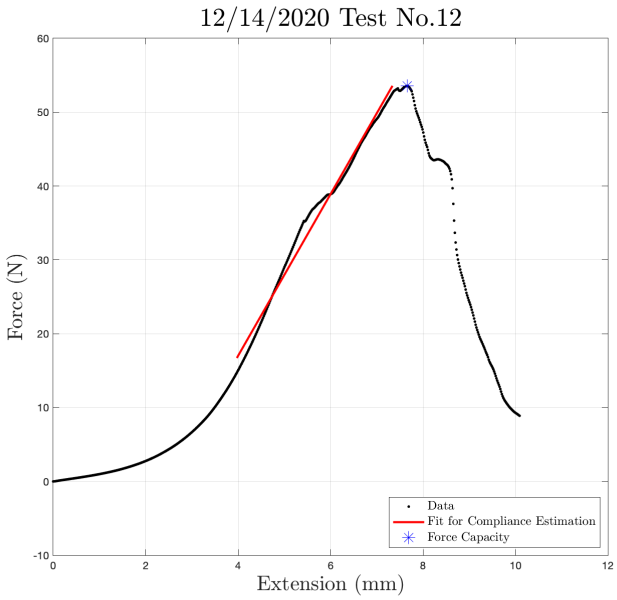
12/14/2020 Test No.12
Force (N)
Extension (mm)
Data
Fit for Compliance Estimation
Force Capacity

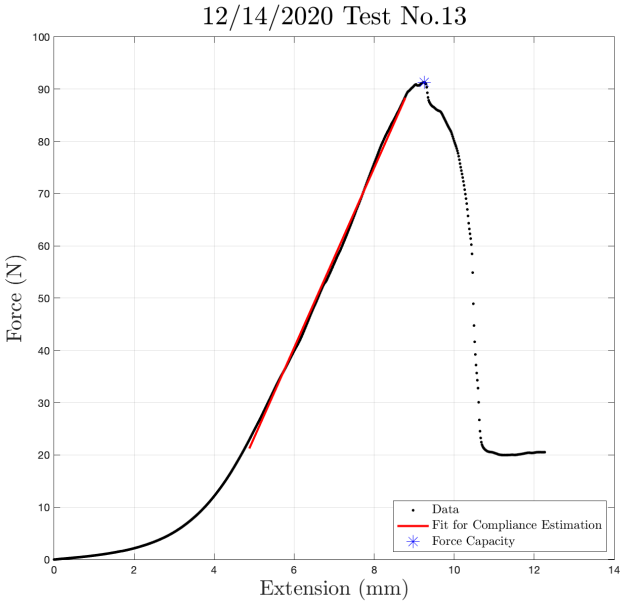
12/14/2020 Test No.13
Force (N)
Extension (mm)
Data
Fit for Compliance Estimation
Force Capacity

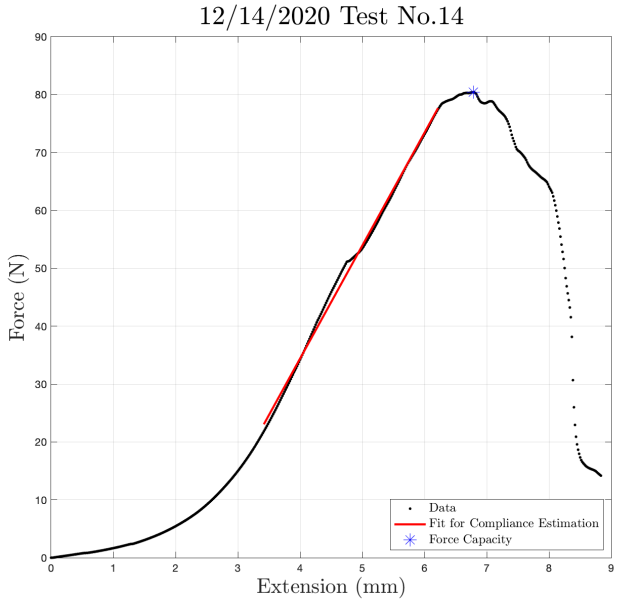
12/14/2020 Test No.14
Force (N)
Extension (mm)
Data
Fit for Compliance Estimation
Force Capacity

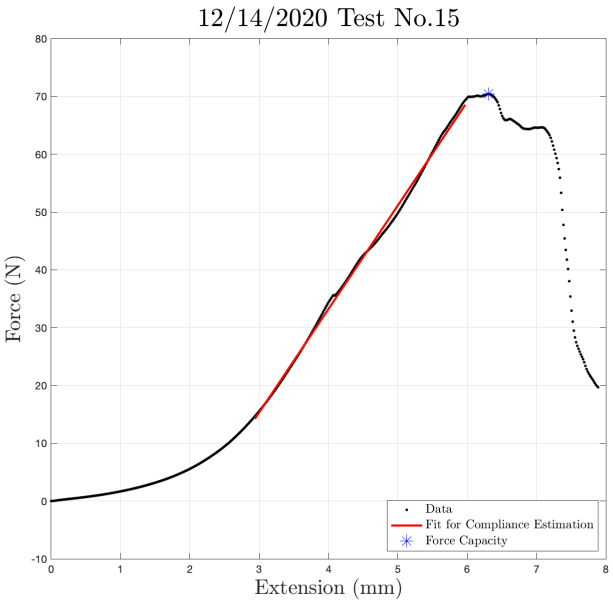
12/14/2020 Test No.15
Force (N)
Extension (mm)
Data
Fit for Compliance Estimation
Force Capacity

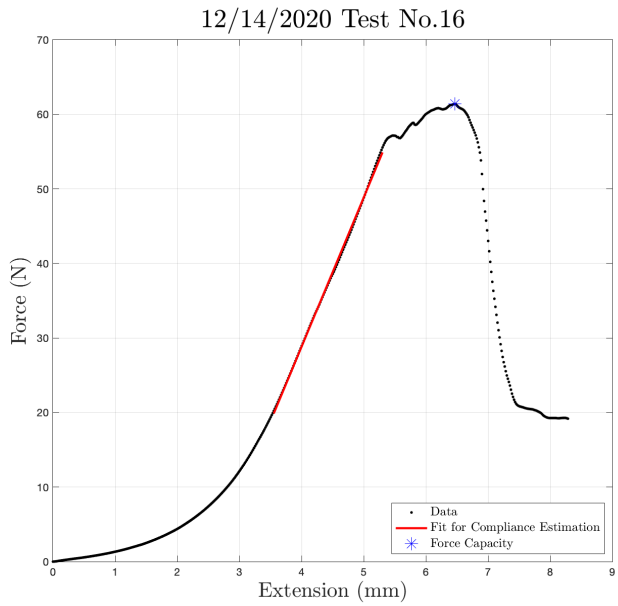
12/14/2020 Test No.16
Force (N)
Extension (mm)
Data
Fit for Compliance Estimation
Force Capacity

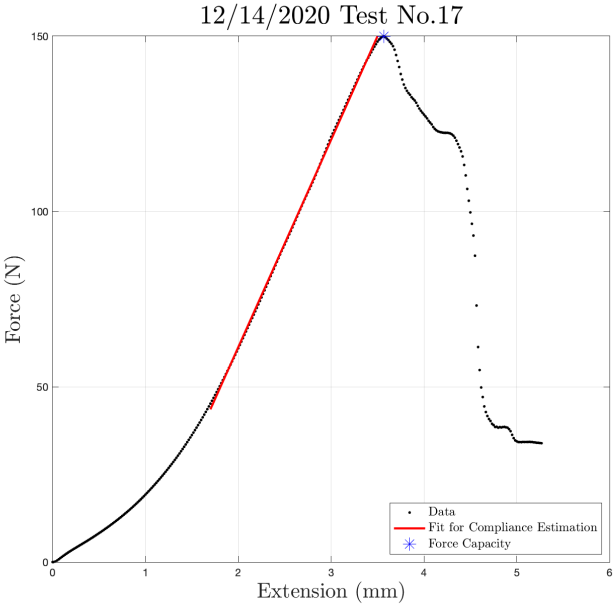
12/14/2020 Test No.17
Force (N)
Extension (mm)
Data
Fit for Compliance Estimation
Force Capacity

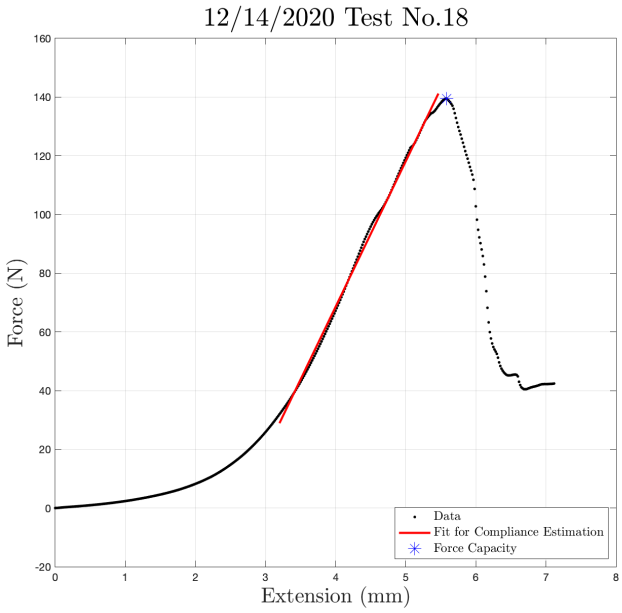
12/14/2020 Test No.18
Force (N)
Extension (mm)
Data
Fit for Compliance Estimation
Force Capacity

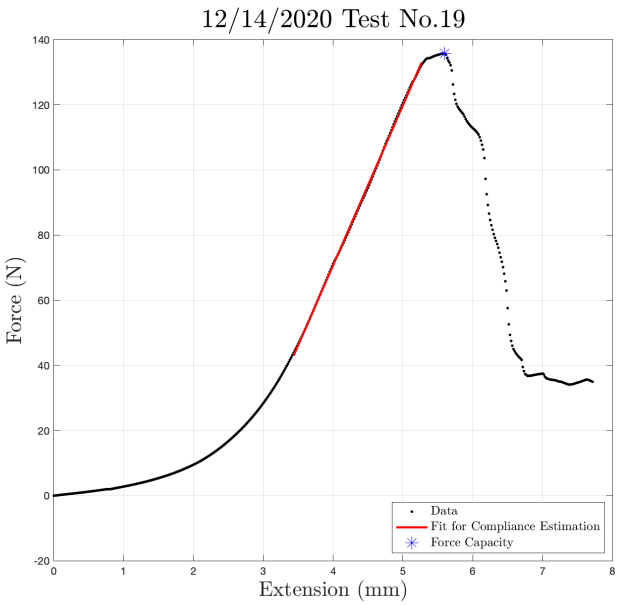
12/14/2020 Test No.19
Force (N)
Extension (mm)
Data
Fit for Compliance Estimation
Force Capacity

Appendix B: Force vs. Extension Plots for Final Tests (76x305 mm pad)

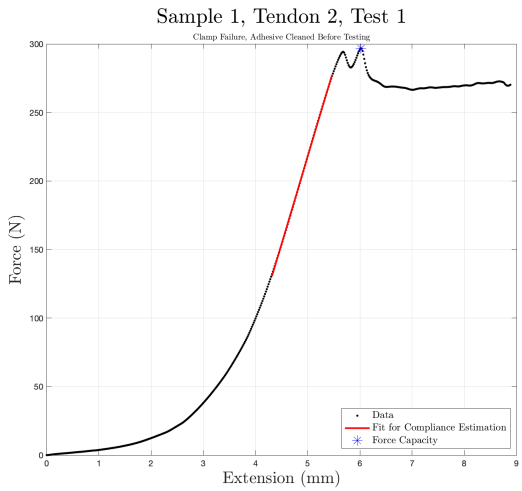

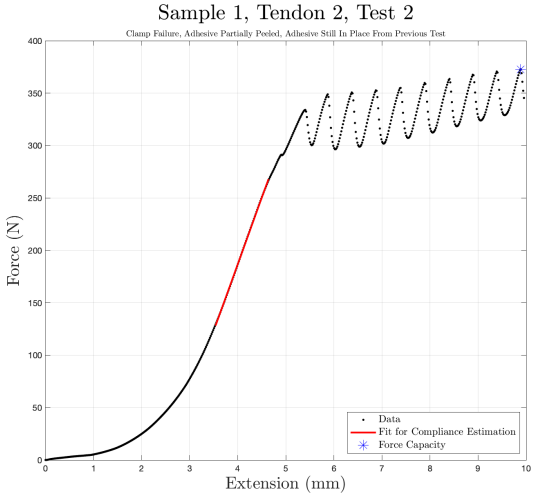

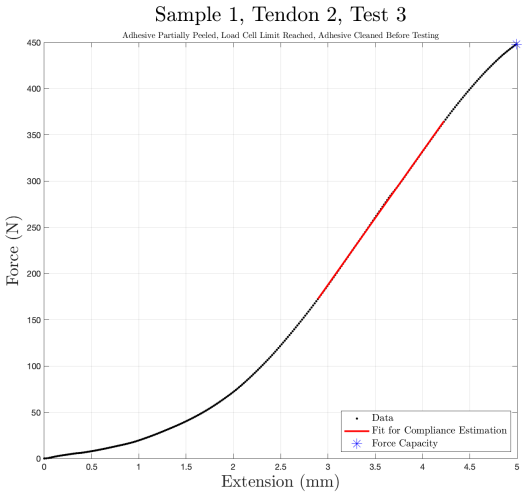

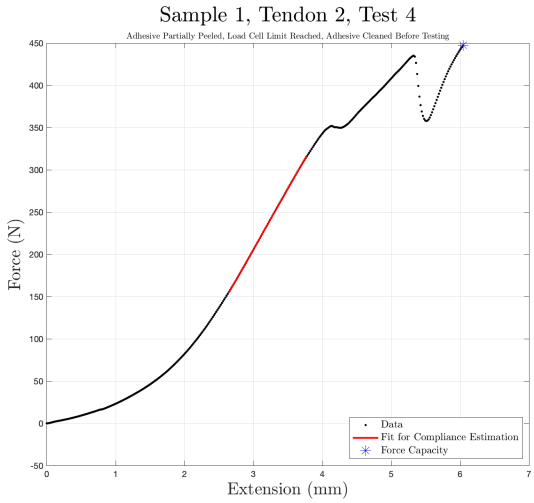

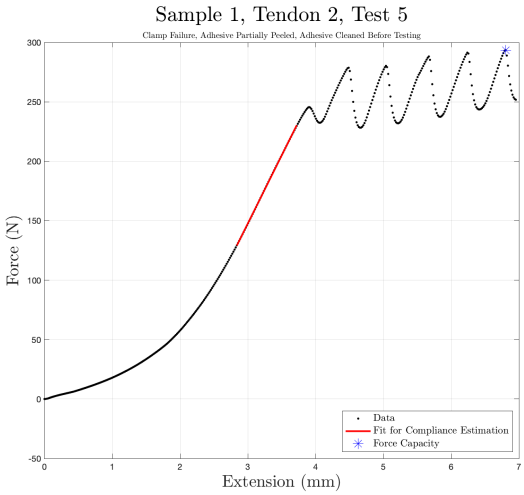

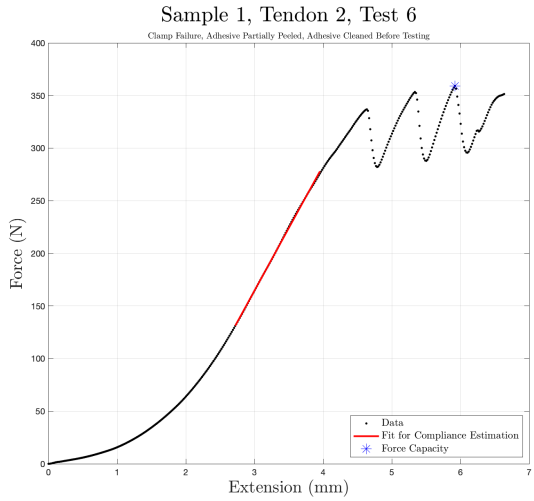

Sample 1, Tendon 2, Test 7

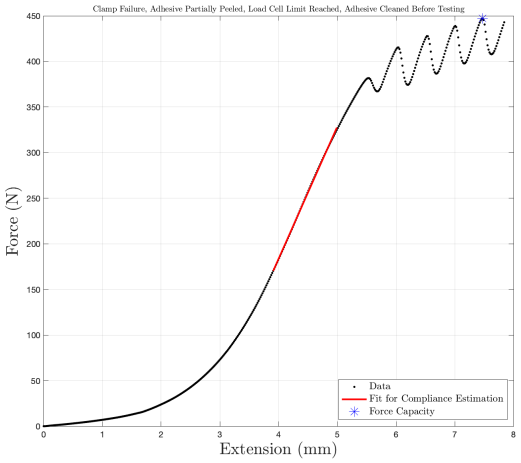

Sample 1, Tendon 2, Test 8

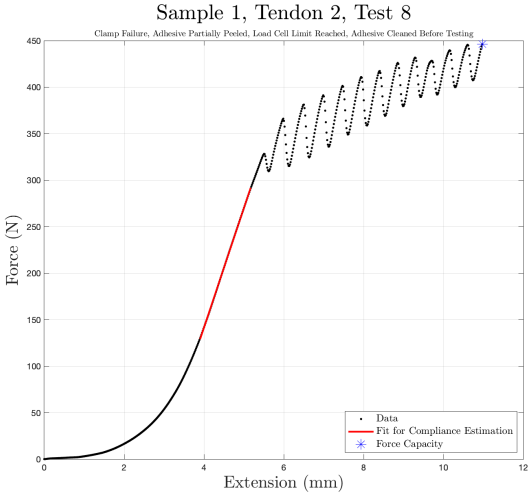

Sample 1, Tendon 3, Test 1

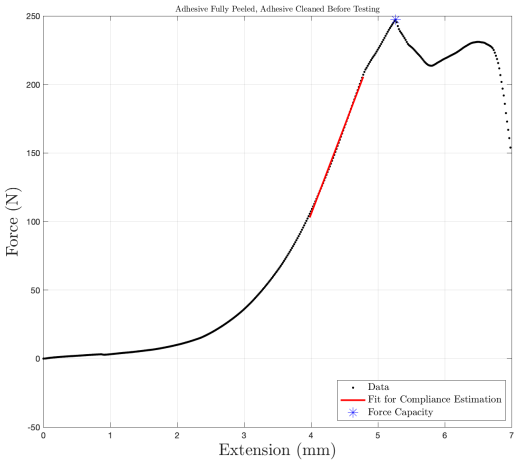

Sample 1, Tendon 3, Test 2

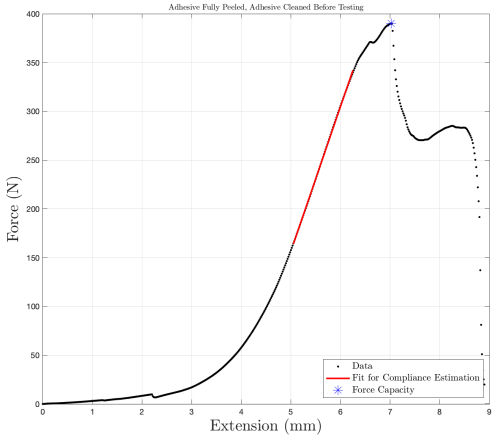

Sample 1, Tendon 3, Test 3

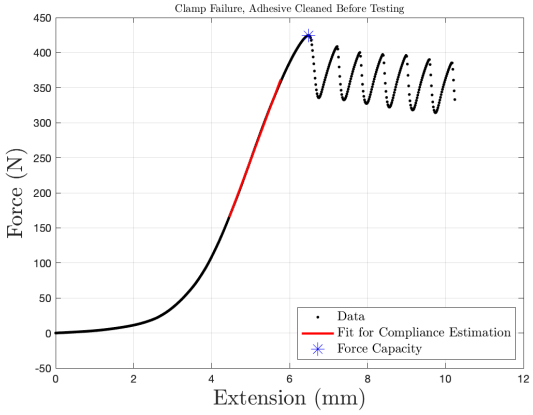

Sample 1, Tendon 3, Test 4

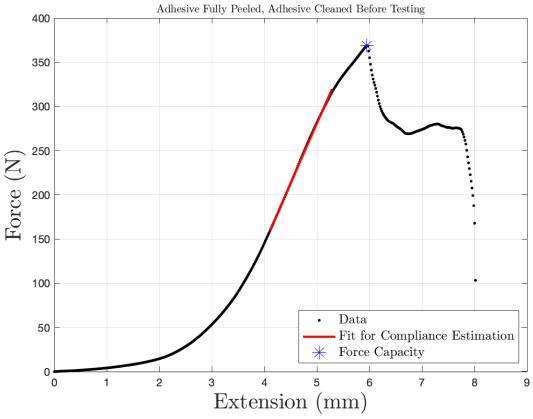

Sample 1, Tendon 3, Test 5

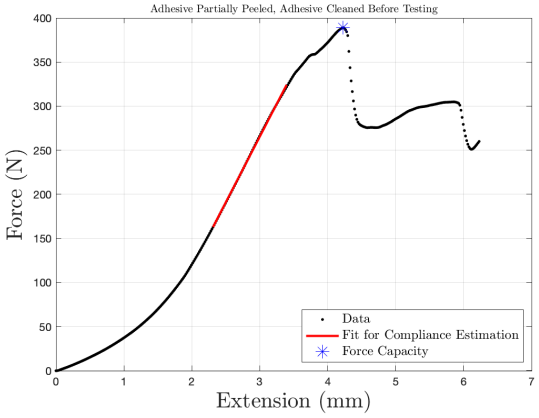

Sample 1, Tendon 3, Test 6

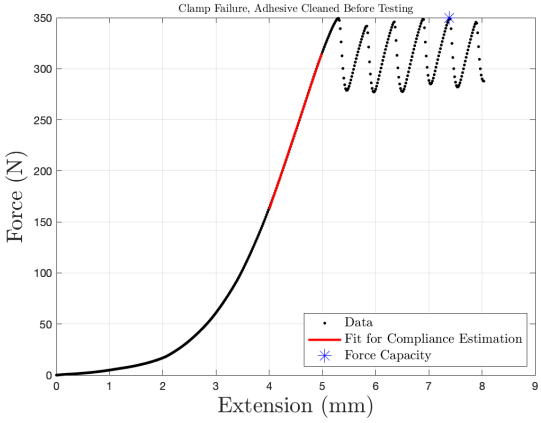

Sample 1, Tendon 3, Test 7

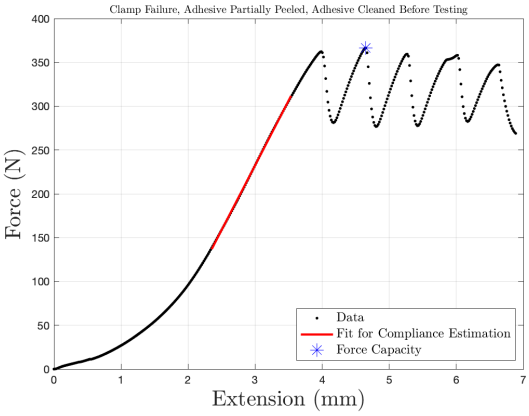

Sample 3, Tendon 2, Test 1

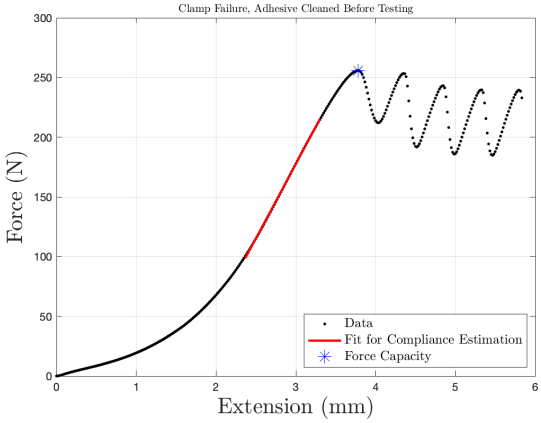

Sample 3, Tendon 2, Test 2

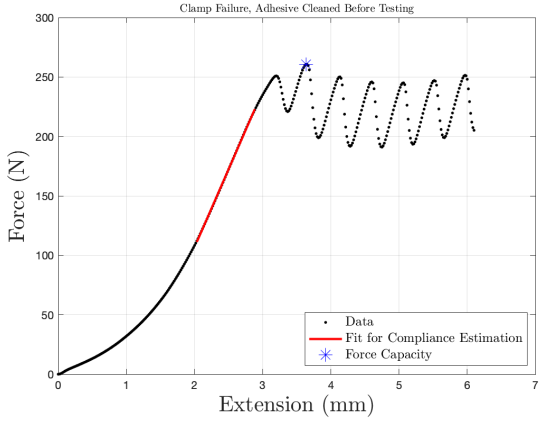

Sample 3, Tendon 2, Test 3

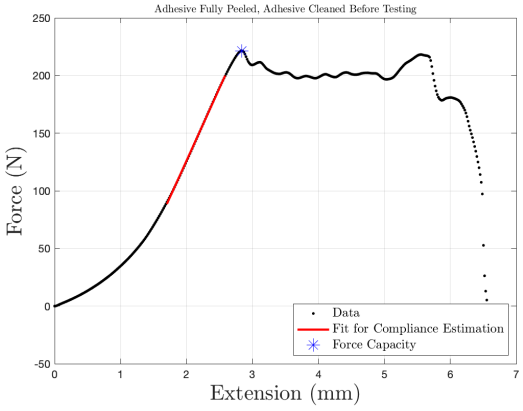

Sample 3, Tendon 2, Test 4

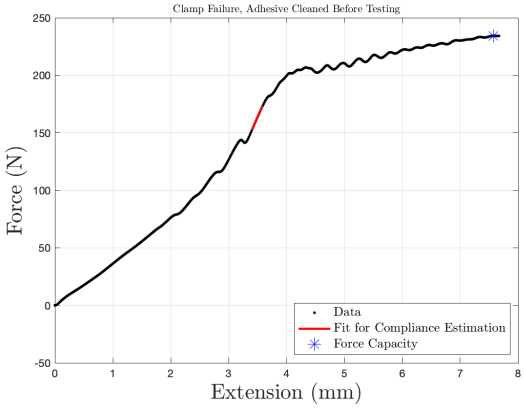

Sample 3, Tendon 2, Test 5

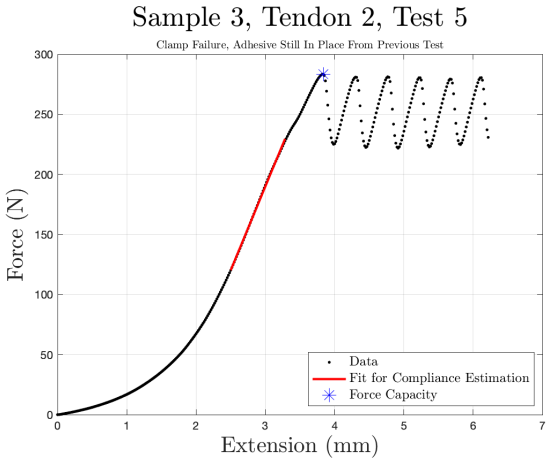

Sample 3, Tendon 3, Test 1

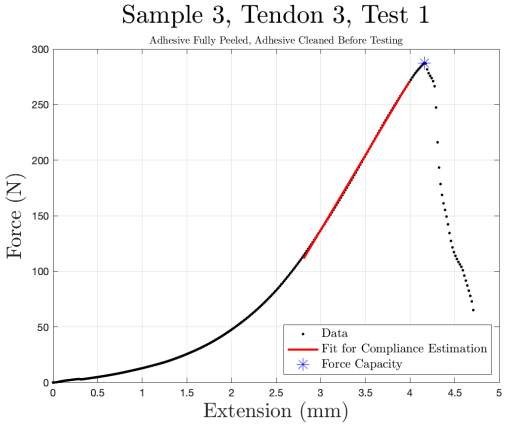

Sample 3, Tendon 3, Test 2

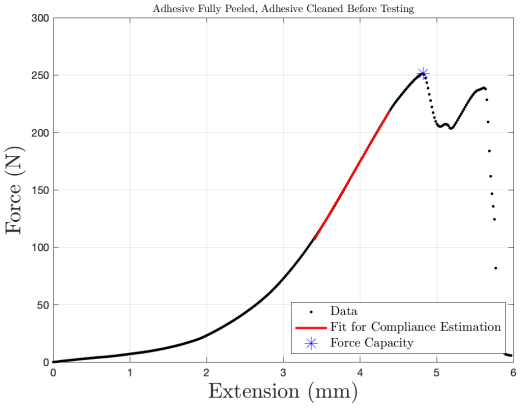

Sample 3, Tendon 3, Test 3

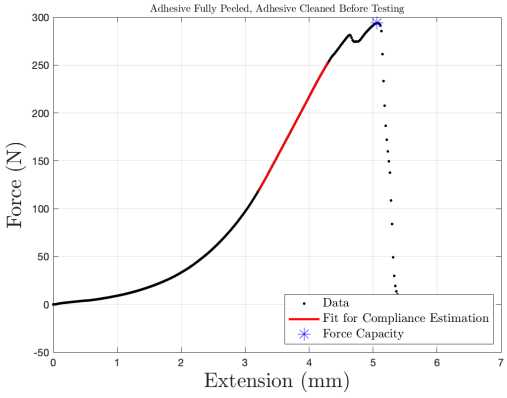

Sample 4, Tendon 1, Test 1

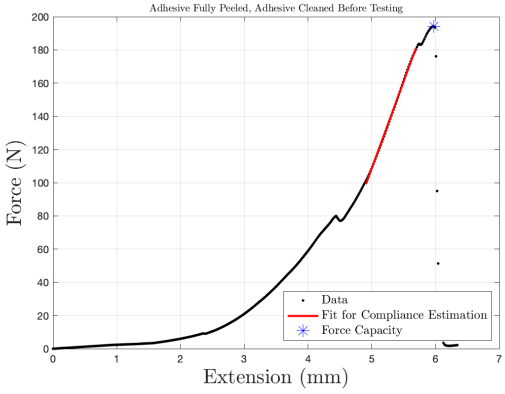

Sample 4, Tendon 2, Test 1

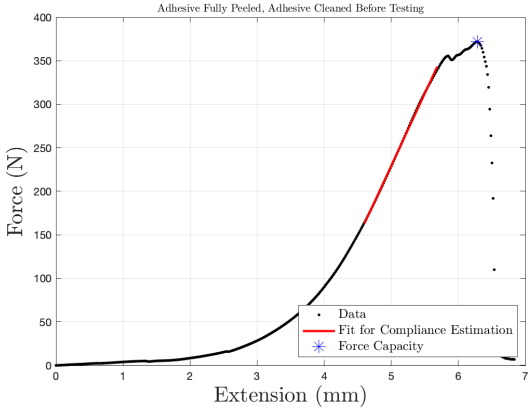

Sample 4, Tendon 3, Test 1

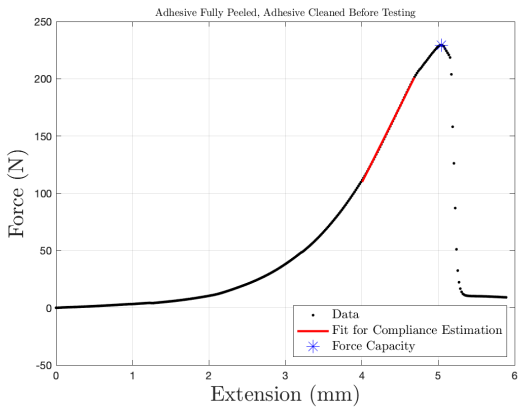

Sample 4, Tendon 4, Test 1

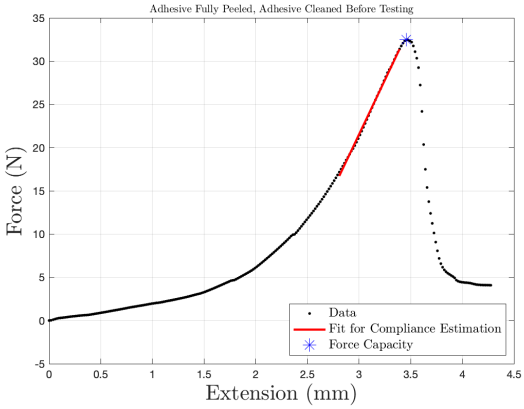

Appendix C: Peeling failure

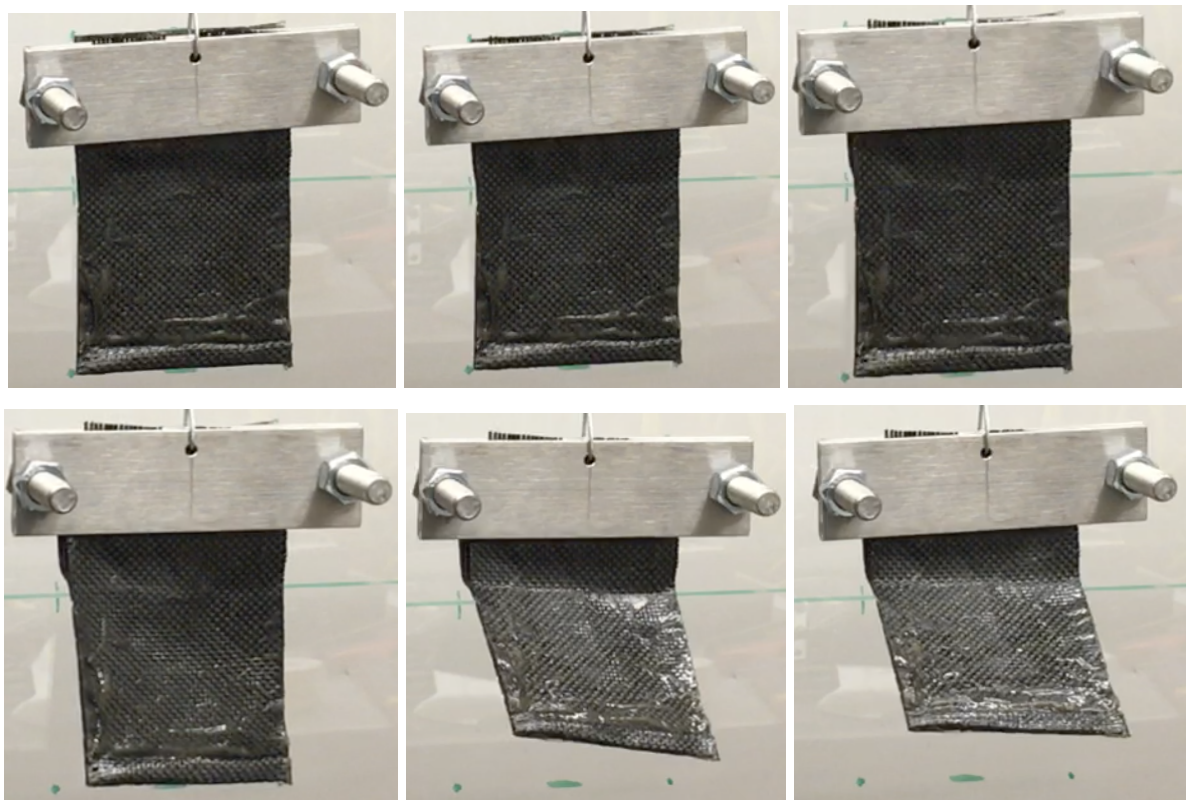

Figure C1. A timelapse of the peeling failure of the adhesive.

Appendix D: Final testing sample images

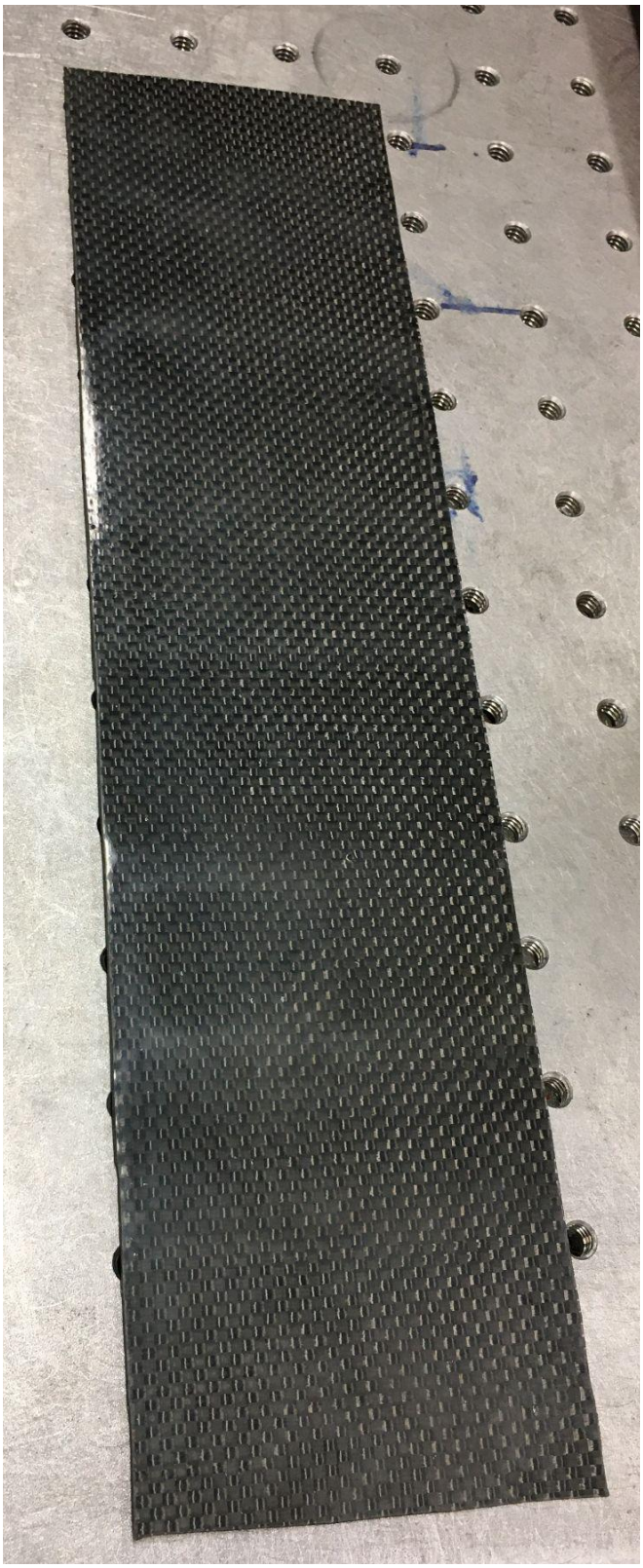

Figure D1. Sample 1

Figure D2. Sample 3

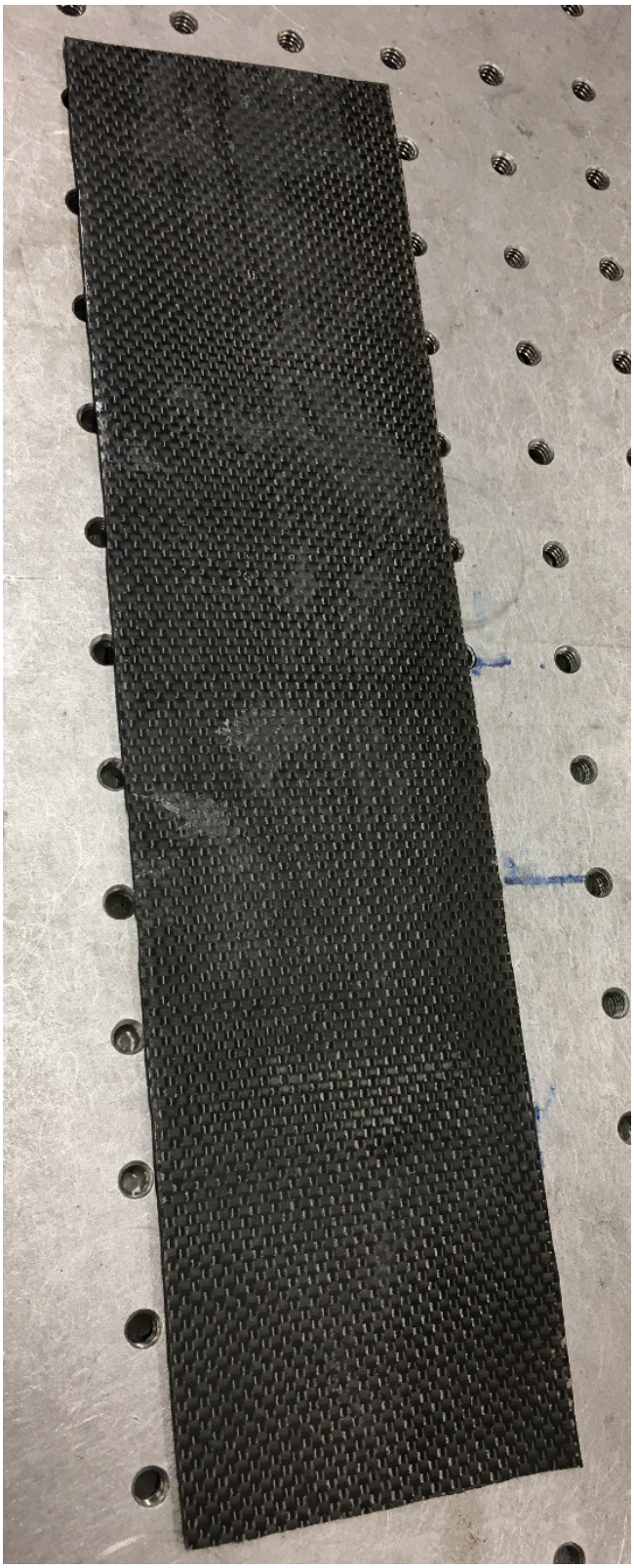

Figure D3. Sample 4